Application of metal and metal oxide nanoparticles@MOFs

Paolo Falcaro[a,*] , Raffaele Ricco[a] , Amirali Yazdi[b] , Inhar Imaz[b] , Shuhei Furukawa[c] , Daniel Maspoch[b,d] , Rob Ameloot[e] , Jack D. Evans[f] , Christian J. Doonan[f,**]

[a] CSIRO Manufacturing Flagship, Private Bag 10, Clayton South, VIC 3169, Australia
[b] Institut Catala de Nanociencia i Nanotecnologia (ICN2), Campus de la UAB, Edifici ICN2 08193 Bellaterra, Spain
[c] Institute for Integrated Cell-Material Sciences (WPI-iCeMS), Kyoto University, Yoshida, Sakyo-ku, Kyoto 606-8501, Japan [d]
Institució Catalana de Recerca i Estudis Avanc¸ ats (ICREA), 08100 Barcelona, Spain
[e] Centre for Surface Chemistry and Catalysis, University of Leuven, Celestijnenlaan 200F, 3001 Leuven, Belgium
[f] Department of Chemistry, School of Physical Sciences, The University of Adelaide, North Terrace Campus, Adelaide SA 5005, Australia

Contents

Keywords:
Composites
Metal-Organic Frameworks
Nanoparticles
Applications
Nanoparticles@MOFs

a b s t r a c t

Composites based on Metal-Organic Frameworks (MOFs) are an emerging class of porous materials that have been shown to possess unique functional properties. Nanoparticles@MOFs composites combine the tailorable porosity of MOFs with the versatile functionality of metal or metaloxide nanoparticles. A wide range of nanoparticles@MOFs have been synthesised and their performance characteristics assessed in molecular adsorption and separation, catalysis, sensing, optics, sequestration of pollutants, drug delivery, and renewable energy. This review covers the main research areas where nanoparticles@MOFs have been strategically applied and highlights the scientific challenges to be considered for their continuing development.

* Corresponding author. Tel.: +61 395452968.
** Corresponding author. Tel.: +61 883135770.
E-mail addresses: Paolo.Falcaro@csiro.au (P. Falcaro), christian.doonan@adelaide.edu.au (C.J. Doonan).

1. Introduction

Metal-Organic Frameworks (MOFs), also called Porous coordination Polymers (PCPs), are of significant interest to chemists due to their exceptionally high surface areas and structural diversity. Furthermore, the modular approach to their synthesis, allows for the preparation of porous networks with precisely tailored chemical and physical attributes [1-5]. These unique features have led researchers to explore combining MOFs with other functional materials to form novel composites with advanced properties [6]. Indeed, ceramics, metal nanoparticles, polymers and biomolecules have been combined with MOFs to afford new materials that have demonstrated unprecedented performance in the areas of catalysis [7], molecular separations [8], sensing [9], plasmonics [10], gas storage [11], controlled guest release [12,13], and protection of biomacromolecules [14]. The most widely studied of these composite systems are based on integrating metal and metal oxide nanoparticles with MOFs. This may be attributed to the versatility of the synthetic approaches for metal oxide (ceramic) and metallic nanomaterials. For example, metal and metal oxide nanoparticles can be prepared by infiltrating the precursors in the pre-formed porous MOF crystals, either via the vapor or liquid phase [1,15]. Particle formation is subsequently triggered within the MOF by the application of heat [16,17], reducing agents [18,19] or radiation [20,21] (Fig. 1a). Alternatively, because the mild synthetic conditions typically used to synthesize MOFs do not affect the chemical composition, structure and morphology of most metal or metal oxide nanoparticles, a 'one-pot' approach can be applied where the MOF is crystallised in the presence of pre-formed functional nanoparticles [22]. In the resulting composite, the MOF encapsulates the functional nanoparticles (Fig. 1b).

A conceptually different, emerging approach termed pseudomorphic replication relies on the preparation of core-shell inorganic particles where the core is the 'functional' nanoparticles and the shell is a feedstock material for the inorganic node of the MOF [13]. Under judiciously controlled conditions, the shell reacts rapidly with the organic precursor ligands to grow the MOF network around the core nanoparticles (Fig. 1c) [23]. Finally, preformed MOFs and nanoparticles can be combined to form clusters of the two components (Fig. 1d).

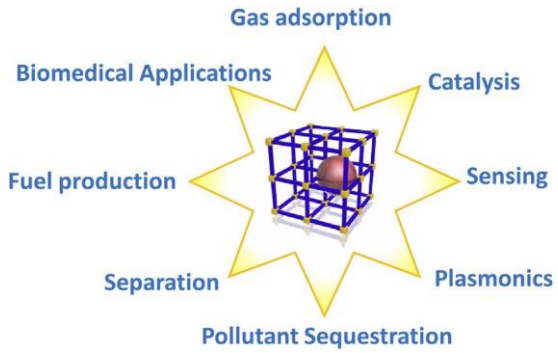

Fig. 2. Schematic illustration of different applications of nanoparticles@MOFs.

The focus of this review is to canvass the variety of applications that have been explored for nanoparticles@MOF composites and to highlight how this unique combination leads to materials with enhanced performance characteristics in the areas of gas adsorption, catalysis, sensing, microelectronics, sequestration, delivery and biomedical applications, fuel production and separation (Fig. 2).

2. NP@MOFs for gas storage and separation

MOFs have been thoroughly investigated for their application to the storage and separation of a number of gases, including hydrogen, carbon dioxide and methane [24-26]. To improve the relatively weak physisorption forces, researchers have applied their efforts

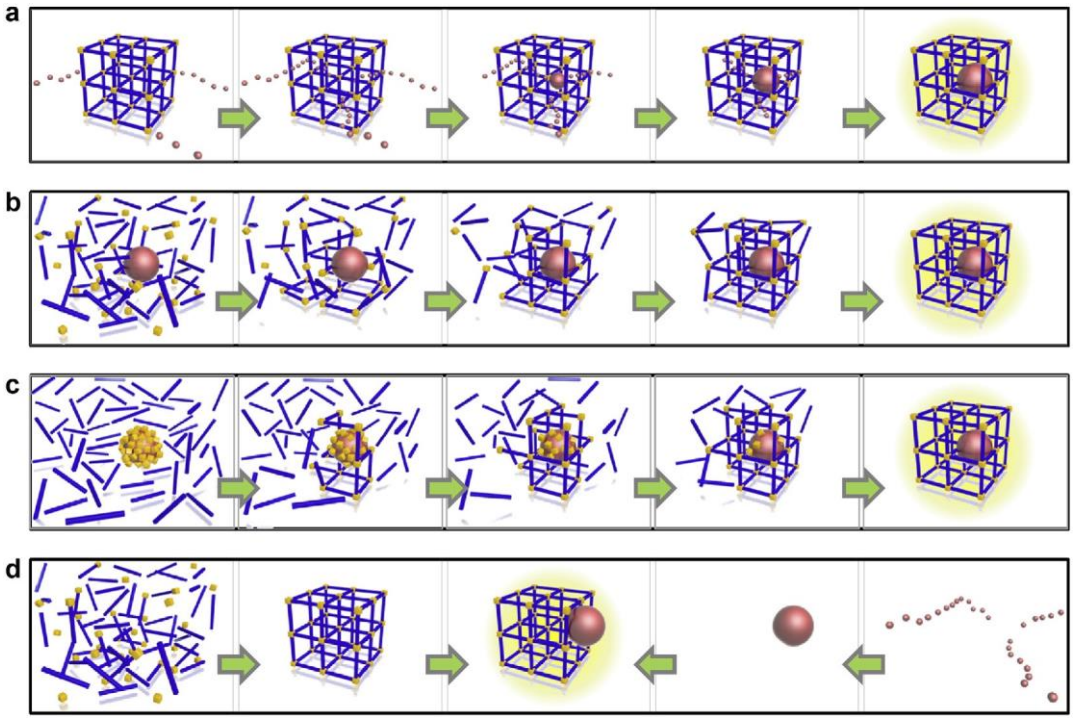

Fig. 1. Different synthetic approaches for the preparation of nanoparticles@MOF composites: (a) infiltration in preformed MOFs, (b) self-assembly of MOFs encapsulating the nanoparticles, (c) pseudomorphic replication converting a ceramic shell of a core-shell nanoparticle into a MOF, (d) individual preparation of MOFs and nanoparticles and subsequent mixing.

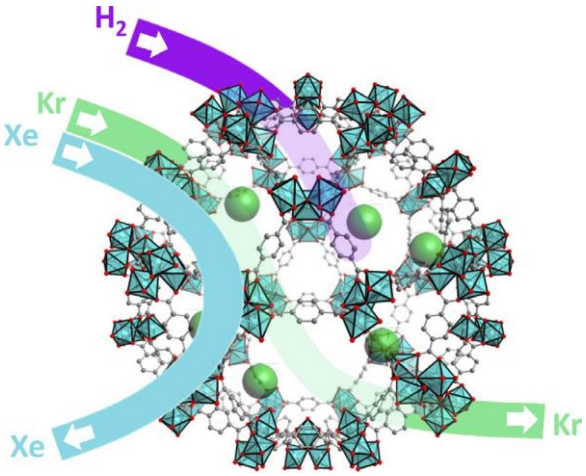

Fig. 3. Schematic illustration of nanoparticles@MOFs for gas adsorption (H_2) and gas separation (Kr and Xe).

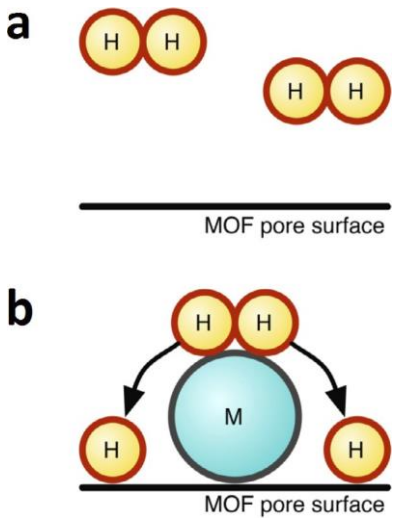

Fig. 4. (a) Hydrogen adsorption on MOFs usually occurs by weak van der Waals interactions. The introduction of metal nanoparticles allows for the stronger mechanism (b) where dissociation and subsequent 'spillover' may occur.

to tuning pore sizes, modifying pore chemistry and generating co-ordinatively unsaturated metal sites [15,27]. In addition, combining metal and metal oxide nanoparticles with MOFs has shown promise towards increasing the interactions with adsorbates that would normally have extremely weak interactions with the pore surfaces such as hydrogen and noble gases. Here we highlight examples where the introduction of nanoparticles into MOFs has been successfully employed to enhance gas adsorption and separation (Fig. 3).

2.1. Hydrogen storage

Alternative energy sources are in high demand given the present concerns of climate change, energy security and pollution. One such alternative is hydrogen gas as it can be produced from domestic resources and can be used to power fuel cells as zero-emission energy generators. Despite the advantages of hydrogen as a fuel source there are concerns over safe storage methods at high pressures, especially for automotive applications. There are a number of strategies that mitigate this issue, one of which is storing hydrogen within porous frameworks. Most porous materials store hydrogen by way of weak van der Waals interactions [28], however, transition metals can adsorb hydrogen via a metallic bonding and dissociation processes, described conceptionally in Fig. 4a. The combination of high surface areas and enhanced adsorption enthalpy at a metal surface suggests that metal/metal oxide@MOF composites are promising materials for hydrogen storage.

An early example of metal/metal oxide@MOF composites for hydrogen storage was reported by Yang and Li who demonstrated that a physical mixture of MOF and Pt supported on active carbon significantly enhances hydrogen uptake capacity at room temperature [29]. Remarkably, the increase in adsorption does not follow the weighted average of MOF and Pt/C. The observed enhancement is attributed to the so-called 'hydrogen spillover' effect (Fig. 4b) where hydrogen molecules dissociate at the metal cluster, then move to the carbon support and subsequently to the organic components of the MOF [30]. This effect has been demonstrated in a number of MOFs [31-35], furthermore, ab initio calculations have been applied in an effort to understand the mechanism of this postulated adsorption process [36-39]. Recently, however, Luzan and Talyzin reported that the spillover effect from Pt/C catalyst to MOF was irreproducible [40], and Hirscher has commented it may be below the detection limit of the gas adsorption apparatus [41]. Yang and co-workers note that the methodology to maximize spillover depends on a number of experimental factors involved in sample preparation [42].

Despite the questionable mechanism of hydrogen spillover in physical mixtures of MOFs with Pt/C, work focused on more structurally well-defined metal nanoparticles@MOF composites has shown promising results. For example, Pd nanoparticles loaded in MOF-5 (1 wt% loading) and in SNU-3 (3 wt% loading) demonstrated increased hydrogen adsorption at low pressure and temperature [43,44]. Pd@SNU-3 also showed an increase in hydrogen uptake at room temperature and high pressure compared to SNU-3, however calculated isosteric heats of adsorption indicated that the Pd@SNU-3 possessed a lower enthalpy of adsorption for H_2. This result further highlights that the mechanism of action in these materials is not comprehensively understood. Materials with significantly higher Pd content have been described by Latrouche and co-workers, who were able to produce MIL-100(Al) embedded with 10 wt% metallic Pd [18]. These high loadings gave rise to a decrease in surface area and pore volume as indicated by nitrogen adsorption experiments. This would be anticipated due to the pore volume consumed by Pd nanoparticles. Consistent with the lower pore volume of these samples, the 77 K hydrogen capacity of the Pd@MIL-100(Al) samples were less than that of the bare framework. However, the room temperature hydrogen uptake capacity was significantly improved; 0.35 wt% at room temperature and 4 MPa. These values are approximately double that of MIL-100(Al). Characterization by X-ray diffraction revealed that the high capacity at room temperature is partially explained by formation of Pd hydride that occurs readily at room temperature. Recently, Kitagawa and co-workers have significantly improved hydrogen storage capacity of Pd nanoparticles by employing a MOF coating [11]. Here, samples of Pd nanocrystals were successfully covered in the HKUST-1 leading to a drastic increase in the storage capacity and kinetics of hydrogen adsorption compared to the base Pd nanocubes (Fig. 5). Notably, at elevated temperatures HKUST-1 shows no appreciable hydrogen adsorption. Further investigations by X-ray photoelectron spectroscopy (XPS) suggest the enhanced hydrogen storage capacity in the composite material is a result of electron transfer from Pd nanocrystals to the HKUST-1 coating. This approach is widely applicable to other metal nanoparticles@MOF systems and may provide a general method to enhance the reactivity of nanoparticles.

Pt nanoparticles are known to afford extremely strong interactions with hydrogen. For example, Pd black is able to absorb and

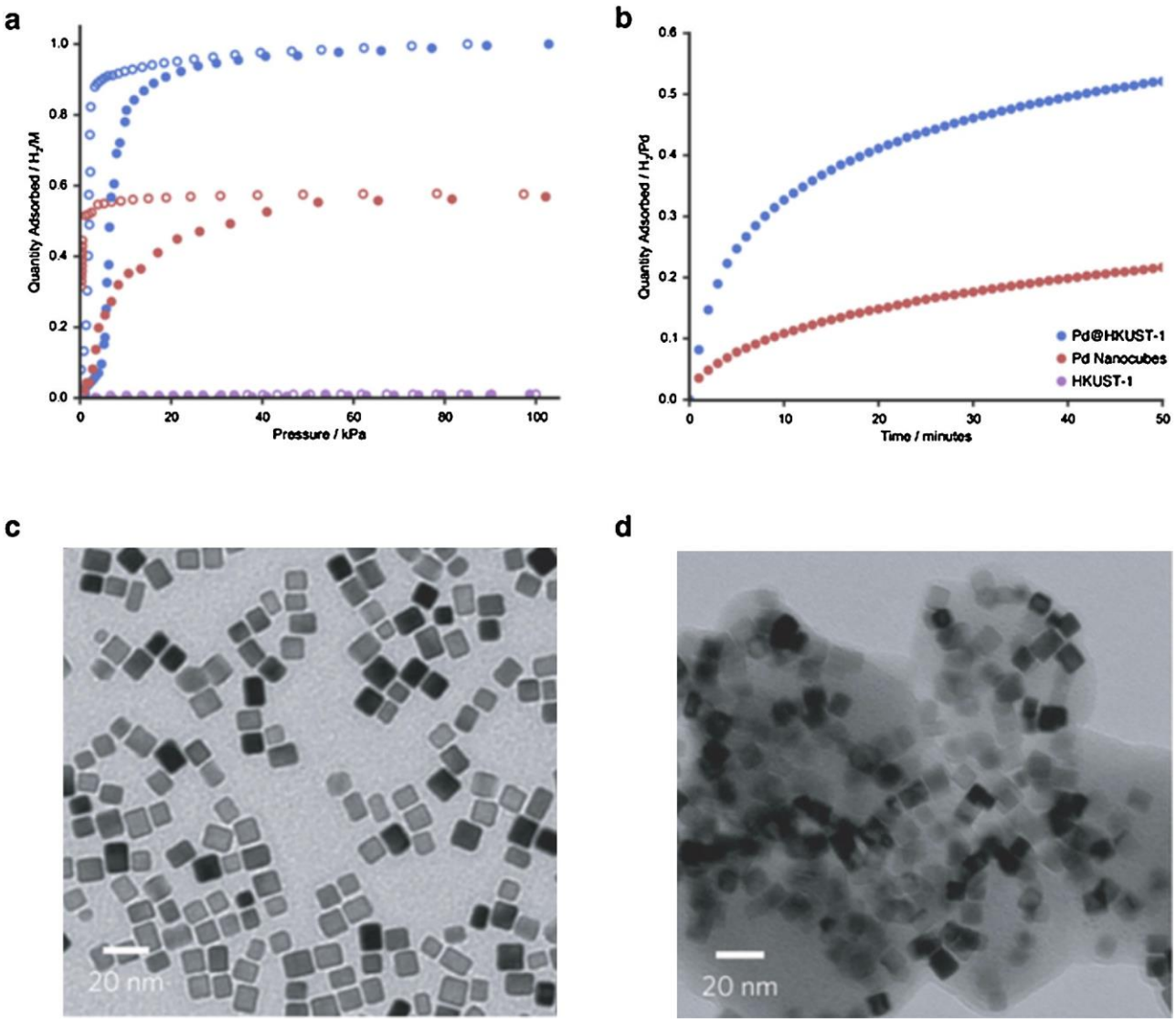

Fig. 5. Hydrogen adsorption isotherms (desorption is shown by open symbols) for bare Pd nanocubes, HKUST-1 and Pd@HKUST-1 at 303 K (a) and hydrogen adsorption profiles at 303 at a pressure of 101.3 kPa over a period of 50 minutes (b). TEM images of Pd nanocubes (c) and Pd@HKUST-1 (d).
Reproduced from ref. [11].

desorb hydrogen at room temperature, however, hydrogen cannot be desorbed from Pt black at room temperature under evacuation [28]. Inspired by the results of Yang and Li's bridged Pt/C and MOF materials [29], Senker et al. were able to synthesize samples of ultra-high surface area MOF-177 loaded with 43 wt% Pt nanoparticles [45]. The resulting composite was reported to adsorb 2.5 wt% of hydrogen at room temperature at 144 bar. This gives rise to a storage capacity of 62.5 g L^{-1}, which is close to that of liquid hydrogen at 70 $g_{H_2} L^{-1}$. Unfortunately, subsequent cycles show decreasing capacity that can be explained by passivation of the Pt surface by stable Pt-H moieties.

Overall, research into hydrogen adsorption in these materials highlights the advantages of combining the strong adsorption potential of metal nanoparticles and high surface areas of MOFs. However, for this area to progress further work needs to be focused on elucidating the mechanism of action for hydrogen adsorption, especially with respect to the observed hydrogen spillover effect [30]. A better understanding of these systems will facilitate the hypothesis driven design of novel composites for H_2 storage.

2.2. Noble gas separation

Molecular separation of Kr and Xe is important as reprocessing nuclear fuel requires the removal of radioactive ^{85}Kr from Xe in the off-gas [46]. Currently, separation of these gasses is achieved by cryogenic distillation. This process is extremely energy intensive owing to the low boiling points of Kr and Xe at −153°C and −108°C, respectively. Similar to hydrogen, noble gases interact very weakly with the surfaces of porous materials. This has motivated researchers to use metal nanoparticles as a strategy towards enhancing uptake capacity. Groose and co-workers reported that Ag clusters in X- and Y-type zeolites gave rise to a higher uptake of Xe, when compared to the original sodium ion containing zeolites, and was dependent on Ag loading [47]. Subsequently, Thallpapally et al. were able to produce Ag nanoparticles in MOF-74(Ni) with up to 6.59 wt% Ag [48]. The Xe and Kr adsorption of these materials showed the Xe capacity at 1 bar and room temperature was increased by 15.6% when compared to the bare framework (Fig. 6). Importantly, the introduction of Ag to MOF-74(Ni) did not significantly increase the Kr capacity, as it is less polarizable than Xe.

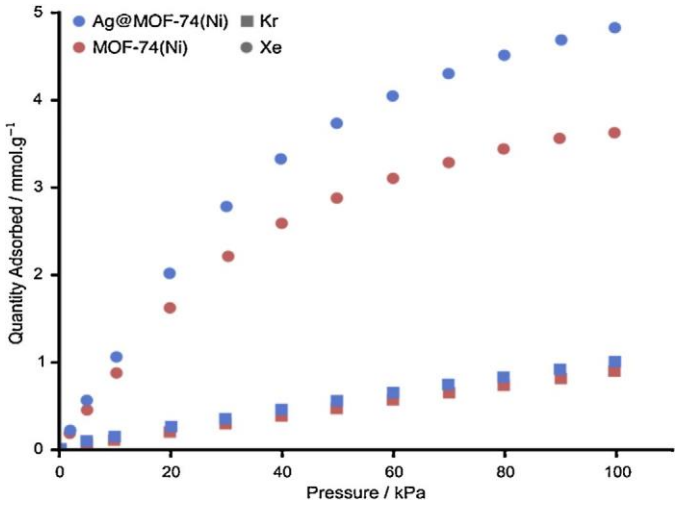

Fig. 6. Xe and Kr isotherms for bare MOF-74(Ni) and a sample of Ag@MOF-74(Ni) loaded with 1.47 wt% Ag.
Reproduced from ref. [48].

Accordingly, the adsorption selectivity (calculated from the pure gas isotherms and a 50:50 mixture) was double that of the benchmark activated-carbon was achieved. These extremely promising results suggest that metal nanoparticle@MOF composites should be further investigated for their potential application to noble gas separations.

3. NP@MOFs for catalysis

Metal nanoparticles are highly attractive materials for catalysis due to the larger surface area/unit volume ratio as compared to their bulk metal analogues that are traditionally used in industrial catalysis [49,50]. However, there are still some major barriers for the widespread use of nanoparticles as catalysts. Some of these drawbacks include a tendency to aggregate, low recyclability, and difficulty recovering the nanoparticles from the reaction media. To overcome these problems, metal nanoparticles are typically immobilized on or in supports [51]. A common strategy is to use porous materials with well-defined pore characteristics; in this way, the partition between the exterior and the interior pore structure permits the selective gating of the molecules that reach, and therefore react with the nanoparticles [52]. Porous materials also have the advantage of confining and protecting the nanoparticles, thus facilitating their recovery from the bulk solution and preventing particle aggregation. In this context, the regular porosity of MOFs together with the possibility to tailor their pore size, shape and chemical functionality makes them an excellent platform to support active metal nanoparticles for heterogeneous catalysis [53].

Table 1 summarizes some reactions already tested using MOF supported metal nanoparticles as catalysts, highlighting the nature of the MOF and the nanoparticle, the nanoparticle size, and the weight percentage of the nanoparticle in the MOF. These studies are largely based on oxidation, hydrogenation, C-C coupling and H_2 production reactions (Fig. 7). However, other important catalytic processes are now being investigated. For example the catalytic synthesis of methanol from CO_2 and H_2, using Cu nanoparticles stabilized into MOF-5, was demonstrated by Fischer et al., who found a maximum 70 $mol_{MeOH}\ g^{-1cat}\ h^{-1}$ methanol production [54]. More recently, complex cascade reactions involving Knoevenagel condensations and subsequent hydrogenations were successfully catalyzed using IRMOF-3 supported Pd nanoparticles [53].

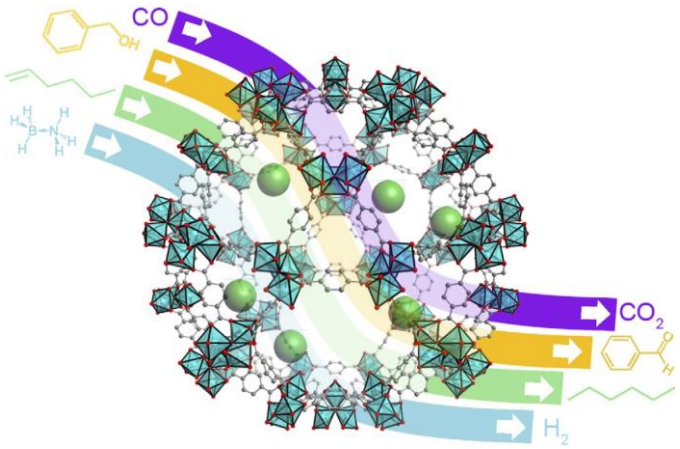

Fig. 7. Schematic Illustration of some representative reactions catalyzed by MOF supported metal nanoparticles.

3.1. Oxidation of CO

Among the oxidation processes, oxidation of carbon monoxide to carbon dioxide has been extensively studied because of the high toxicity of carbon monoxide and its importance in fuel cell technology, where the preferential oxidation of carbon monoxide in excess of hydrogen is a key process for the production of clean fuel [55]. Overall, MOF supported nanoparticles have showed good performance for carbon monoxide oxidation at elevated temperatures. For example, Xu, Hupp, and Gascón groups reported that Au and Pt nanoparticles supported in ZIF-8 and NH_2-MIL-101(Al) afford the total conversion of carbon monoxide to carbon dioxide at around 200°C [7,56,57]. Importantly, the reaction temperature can be reduced to 100-150°C by incorporating Pt, Pd and Cu nanoparticles within MIL-101 and Pd nanoparticles within MOF-5 [58-60]. Additionally, the total conversion of carbon monoxide to carbon dioxide was observed when CuO/CeO_2 nanoparticles were formed, in situ, within HKUST-1 [61].

3.2. Oxidations of alcohols and hydrocarbons

MOF supported metal nanoparticles have been also used as catalysts for aerobic alcohol oxidation reactions which are considered as key reactions in 'green' organic synthesis. These processes usually require temperatures above 100°C (under solvent free conditions), or the presence of a large excess of a base. The majority of these investigations employ Au and Pd nanoparticles supported in different MOFs. Fischer and co-workers first studied the oxidation of benzyl alcohol to benzyl aldehyde using Ru and Au nanoparticles [62], and Au/ZnO and Au/TiO_2 nanoparticles [63] supported on MOF-5. For the Ru nanoparticles, which could be easily converted to RuOx by oxidation with diluted O_2 gas inside MOF-5, the conversion of benzyl alcohol was low (25%). This was attributed to the structural decomposition of MOF-5 during the oxidation reaction. However, in the case of Au and hybrid Au/ZnO and Au/TiO_2 nanoparticles, the authors observed better performance (conversion ranges of 50-70%) when a base was added to accelerate the oxidation reactions by deprotonation of the alcohol. These results were in contrast to those obtained by Ishida et al., who reported that Au nanoparticles embedded in MOF-5 activate the oxidation reaction with base (conversion = 100%) but also without base (conversion = ~70%) [64].

A variety of alcohol oxidation reactions have been investigated by the group of Li. Here, catalytic activity of a series of composites was assessed that were made from different combinations of MOFs (DUT-5, UiO-66, MOF-253, UiO-67, and MIL-101(Cr))

Table 1
List of MOF supported metal nanoparticle catalysts by reaction and substrate.

MOF composite	Nanoparticle	Weight (%)	Size (nm)	Conv. (%)[a]	Ref.
Oxidation					
CO					
ZIF-8	Pt	3.4	2.5 ± 4.1	100	[7]
ZIF-8	Au	5	4.2 ± 2.6	100	[56]
MIL-101-NH_2 (Al)	PTA/Pt			100	[57]
MIL-101(Cr)	Cu/Pd	2.9	2-6	100	[58]
MIL-101(Cr)	Pt/Pd	2.9	3-9	100	[59]
MOF-5	Pd	0.19		65	[60]
HKUST-1	CuO/CeO_2		5-15	100	[61]
MIL-101(Cr)	Pt	2/1/5	1.8 ± 0.2	100	[99]
Ra-MOF	Pd	3.6	1.8 ± 0.3	100	[100]
Alcohols					
MOF-5	Ru	30	1.5-1.7	25	[62]
MOF-5	Au/ZnO-Au/TiO_2 -Au	1-20	2.7-20	50/68/74	[63]
MOF-5/MIL-53(Al)	Au		1.5 ± 0.7	99	[64]
DUT-5/UiO-66/MOF-253	Pt	0.5	1.5-2	99	[65]
UiO-67	Pd	1	3±0.5	99	[66]
MIL-101(Cr)	Au	0.5	2.3 ± 1.1	100	[67]
ZIF-8	Au	30	3.7	81	[68]
UiO-66-$NaBH_4$	Au		5-7	94	[69]
MOF-177	Pt	43	2-3		[45]
UiO-66-NH_2	Au	1.8	2.8-3.1	94	[101]
UiO-66	Au	8		54	[102]
MIL-101(Cr)	Pd	0.35	2.5 ± 0.5	99	[103]
Cyclohexane					
MIL-101(Cr)/MIL-53(Cr)	Au	4.64/4.63	4.8 ± 2.9	30/31	[70]
MIL-101(Cr)	Au/Pd	1	2.4 ± 0.6	51	[71]
Benzylic hydrocarbons					
HKUST-1	Fe_3O_4	28.78	20		[72]
Benzyl-amine					
UiO-66-$NaBH_4$	Au	5-7		53	[69]
Ethylene					
ZIF-8	Pt/Pd	4.95/2.70	6.2	94	[73]
Hydrogenation					
Ketones					
MIL-101(Cr)	Pt		1.5-2.5	97-98	[85]
MIL-101(Cr)	Pd	15	2-3.5	100	[86]
MIL-101(Cr)	Pd	42-45	1.7	100	[89]
1-Hexene					
ZIF-8	Pt	0.23-0.74	2-3	95	[83]
1-Hexyne					
ZIF-8	Pt	1	2.7	100	[84]
1,4-Butynediol					
ZIF-8	Pd	5	4-6	98	[104]
Styrene					
MIL-101(Cr)	Pd	1	1.5	80-100	[82]
MOF-5	Pt	1		97	[43]
MesMOF-1	Ni	20	1.1	99	[105]
Toluene					
MIL-101-NH_2 (Al)	PTA/Pt				[57]
Acetylene					
MIL-101(Cr)	Pd	1	1.5	80-100	[82]
Nitroarenes/Nitrobenzene					
MIL-101(Cr)	Pt	1	1.5-2.5	100	[88]
MesMOF-1	Ni	20, 35	1.1, 1.4-1.9	100	[105]
Phenol					
MIL-101(Cr)-MIL-53(Cr)	Pd	4.3/4.9	2.5/4.3	100	[87]
Nitrophenol					
ZIF-8	Au	10-15	2-3	100	[106]
ZIF-8	Au/Ag	2/2		100	[107]
MIL-100(Fe)	Au			100	[108]
Cyclohexanone/Cycloheptanone					
MIL-101	Ni/Pd	18	2.5-3.5	80/100	[109]
Octane					
MIL-101(Cr)	Pt	1.2	5±0.5	100	[90]

Table 1 (Continued)

MOF composite	Nanoparticle	Weight (%)	Size (nm)	Conv. (%)[a]	Ref.
2,3,5-trimethylbenzoquinone					
MIL-101(Cr)	Pd	2	2-3	100	[91]
Benzene/cyclohexene					
MOF-5	Ru	0.98	2	99	[110]
Other olefins					
HKUST-1	Au/Pt		100	25	[111]
2.16. Vanilin					
MIL-101(Cr)	Pd	2	1.8 ± 0.2	45	[112]
Dehalogenation of aryl chlorides					
MIL-101-NH_2 (Cr)	Pd	0.62	2.49	98	[92]
C-C coupling					
Suzuki-Miyaura coupling					
MIL-101(Cr)	Pd	1	1.9 ± 0.7	82	[93]
MIL-53-NH_2 (Al)	Pd	1	3.12	99	[94]
MIL-101-NH_2 (Cr)	Pd	8	2-3	99	[95]
MCoS-1	Pd	1	2-3	97	[96]
Ullman coupling					
MIL-101(Cr)	Pd	1	1.9 ± 0.7	99	[93]
Sonogashira reaction					
MCoS-1	Pd	1	2-3	94	[96]
MOF-5	Pd	3	3-6	100	[97]
Heck reaction					
MIL-53-NH_2 (Fe)	Pd	0.96	3.2	83	[98]
Hydrogen generation					
IRMOF-3	Pd	2	35	100	[53]
MIL-101(Cr)	Ni/Au		1.8 ± 0.2	100	[74]
ZIF-8	Ni	19	2.7 ± 0.7	100	[75]
ZIF-8	Ni/Pt	1-3	2.2 ± 0.3	100	[76]
MIL-101-EDA(Cr)	Au/Pd	13.7/1.5	2-3	100	[77]
MIL-125-NH_2	Pd	0.5	3.1		[78]
MIL-101-NH_2 (Cr)	Pt	1.5	3.75 ± 0.5		[79]
HKUST-1	Pd	0.86	4.3 ± 1.1	100	[113]
Other					
Reduction of Cr(VI)					
UiO-66-NH_2	Pd	0.93	3-6	100	[114]
MIL-101(Cr)	Pt	2	2.6	100	[115]
Methanol synthesis					
MOF-5	Pd/Cu	36/13	1-2		[54]
MOF-5	Cu/ZnO	1.4/40	1-3		[116]
Conversion of methylcyclopentane					
UiO-66	Pt	0.4	2.5	100	[117]
Synthesis of arylamines					
MIL-101(Cr)	Pd/Pt				[118]
Aminocarbonylation					
ZIF-8	Pd	1	4-9	99	[119]
MOF-5	Pd	1	3-12	92	[120]
Indole synthesis					
MIL-101(Cr)	Pd	3	2.6	67	[121]
Phenylation of naphthalene					
MOF-5	Pd	2.3	20	65	[122]
Direct arylation					
MIL-101(Cr)	Pd	0.5	2.6 ± 0.5	85	[123]

[a] Maximum conversion value reached (or reported).

and metal nanoparticles (Pt, Pd and Au). Overall, they showed that the confined metal nanoparticles were highly active in this type of oxidations under base free conditions (conversions up to 100%). The authors attributed these results to the electron donation and confinement effects offered by MOFs [65-67]. Other systems including Au nanoparticles supported in ZIF-8 and UiO-66 and Pt nanoparticles supported in MOF-177 also showed very good catalytic activity for the conversion of alcohols to aldehydes [44,68,69].

Beyond alcohols, the oxidation of hydrocarbons has also been catalyzed using MOF supported nanoparticles. Hydrocarbons have been selectively oxidized, with molecular oxygen as the oxidant, by Au, Au/Pd, Fe_3O_4 or Pt/Pd nanoparticles immobilized in several MOFs (MIL-101 (Cr), MIL-53 (Cr), HKUST-1 and ZIF-8) [70-73]. For example, Huang et al. studied the activity of ZIF-8 supported bimetallic Pt/Pd nanoparticles for the photoactivated oxidation-degradation of ethylene to CO_2 and H_2O [73]. This nanocomposite showed excellent synergistic photocatalytic activity (conversion = 94%), which was to the authors contend due to the fact that ZIF-8, in addition to serving as a support to prevent particle aggregation, has an excellent capacity to adsorb ethylene and thus promote its photodegradation to CO_2 and H_2O.

3.3. Hydrogen generation

One of the biggest challenges in chemistry today is the energy efficient generation of H_2. With this goal in mind, Xu and co-workers evaluated the activity of Au, Ni and hybrid Au/Ni nanoparticles in MIL-101 and of Ni nanoparticles in ZIF-8 for the catalytic dehydrogenation of ammonia borane to generate H_2. In this case complete dehydrogenation was observed [74,75]. Other reactions for hydrogen production have also been evaluated. Singh and Xu successfully studied the generation of H_2 by decomposition of hydrazine in aqueous solution using ZIF-8 supported Ni-Pt bimetallic nanoparticles [76]. In addition, the same group and Martis et al. proved that it was possible to catalyze the dehydrogenation of formic acid using bare and amine-functionalized MIL-101-ethylenediamine supported Au-Pd bimetallic nanoparticles [77] and amine-functionalized MIL-125 supported Pd nanoparticles [78]. Recently, water splitting to produce H_2 using Pt nanoparticles embedded into MIL-101-NH_2 (Cr) was also evaluated. A maximum turnover of 110 mol_{H_2} mol^{-1}_{cat} wasachievedwhenthe loading of Pt nanoparticles was 0.5% [79]. Finally, the photocatalytic properties of Pt@MOFs were also tested for H_2 production. Here, Lin's group first studied the photocatalytic performance of Pt nanoparticles embedded into two UiO frameworks functionalized with $[Ir(ppy)_2(bpy)]^+$ (where ppy is 2-phenyl-pyridine and bpy is 2,2′-bipyridine) complexes, and found that high Ir-based turnover numbers [defined as n(1/2H_2)/n(Ir))] of 3400 and 7000 were achieved when irradiated under visible light (>420 nm). Under these conditions, the $[Ir(ppy)_2(bpy^{\bullet-})]$ radicals generated by triethylamine-mediated photoreduction could transfer electrons to Pt nanoparticles to reduce protons for H_2 production [80]. Also, Matsuoka's group found that Pt nanoparticles photodeposized on amino-functionalized MIL-125(Ti) were able to photocatalyze the generation of H_2, reaching a total production of 33 mol H_2 when this system was immersed in an aqueous solution containing triethanolamine at room temperature while being subjected to visible-light (>420 nm) for 9 h. In this case, the reaction proceeded through the light absorption by the organic linker forming the MOF followed by the electron transfer to the photocatalytically active titanium-oxo cluster. In this system, Pt nanoparticles acted as cocatalysts [81].

3.4. Hydrogenation of olefines

A fourth vast family of catalytic reactions studied using MOF supported metal nanoparticles as catalysts is the hydrogenation of alkenes [82,83], alkynes [82,84], ketones [85,86], and aromatics [43,82,87]; all of which are key processes in chemical industry. As can be seen in Table 1, the most active metal nanoparticles for these reactions are Pt and Pd, and the most promising MOF support is MIL-101 most probably due to its stability and large pore channels. Using this combination, excellent conversion rates (~100%) for the hydrogenation of ketones, aromatic molecules, alkenes, alkynes and nitro compounds have been observed [82,85-92].

3.5. Carbon-carbon coupling

Finally, the last ensemble of reactions that have been catalyzed by MOF supported NPs concern the C-C coupling reactions. Such transformations include Suzuki-Myaura [93-96], Sonogashira [96,97], Ulmann [93], and Heck [98] reactions. Compared to other metal nanoparticles, Pd offers undoubtedly the best conversion rates in C-C coupling and thus Pd@MOF composites are primarily tested for these types of catalytic reactions. An illustrative example was reported by Yuan et al., who developed a very efficient Pd@MIL-101(Cr) catalyst for water mediated Suzuki-Miyaura and Ullmann coupling reactions. This catalyst showed high stability,

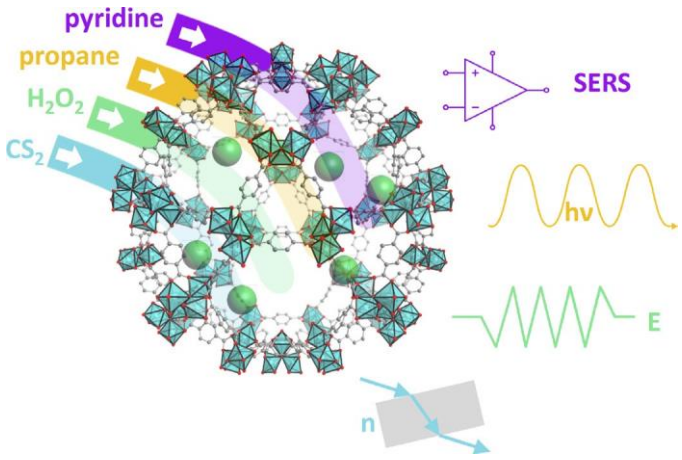

Fig. 8. Schematic illustration of Nanoparticles@MOFs for sensing different analytes (left side) entering in the frameworks. The analyte, as a host, interacts with the composite that could amplify the Raman signal (SERS), affect the luminescent properties, induce changes in the electrical or optical (refractive index) properties.

low metal leaching and high activities (conversion = 100%) over a large number of cycles [93].

4. NP@MOFs for sensing

A wide range of applications, including chemical threat detection, medical diagnostics, food/drink quality control, explosives and pollutants detection, requires sensors that detect specific molecules or elements with high selectivity, sensitivity, and speed of analysis [124-126]. Typical transduction mechanisms are changes in the electrical, photophysical or mechanical properties of the sensor material when it interacts with the analyte (sensing, Fig. 8). Metal nanoparticles have been widely investigated as sensor components because their physical properties (mainly optical, electrochemical or photoelectrochemical) are readily modulated upon interaction with molecules [127,128]. Recently, MOFs have been proposed as a novel class of support for chemical probes, as pre-concentrators, and as molecular filters and templates. In this respect, MOFs act in an analogous way to other porous materials, such as mesoporous silica or zeolites. However, MOFs offer greater possibilities for tailoring the pore size and chemistry in order to enhance the adsorption of targeted molecules or elements [129].

4.1. Size-selective sensors

One of the most promising strategies for designing highly selective/sensitive sensors is to synthesize metal/metaloxide MOF composites in order to combine their complementary properties [130]. To date, most of these sensors are constructed by embedding metal nanoparticles in the MOF crystals. Thus, the working mechanism relies on the target molecule diffusing to the embedded metal nanoparticles, through the MOF pores, where interaction causes a detectable change in physical properties. According to this mechanism, the properties of the MOFs are expected to play a major role on the final performance of the sensor. For example, the uniform pore size and resulting size-selectivity of MOFs enabled the development of sensors in which the MOFs act as size-exclusion filters [131]. A pioneering example of this type of sensors was recently reported by Sugikawa et al. [10], who synthesized a MOF-5 supported Au nanorod sensor that showed Surface-Enhanced Raman Scattering (SERS) behavior when contacted with certain pyridine derivatives (Fig. 9a). SERS is a powerful vibrational spectroscopy technique that allows the detection of sub-attomolar quantities of analyte due to the million-fold Raman scattering enhancement

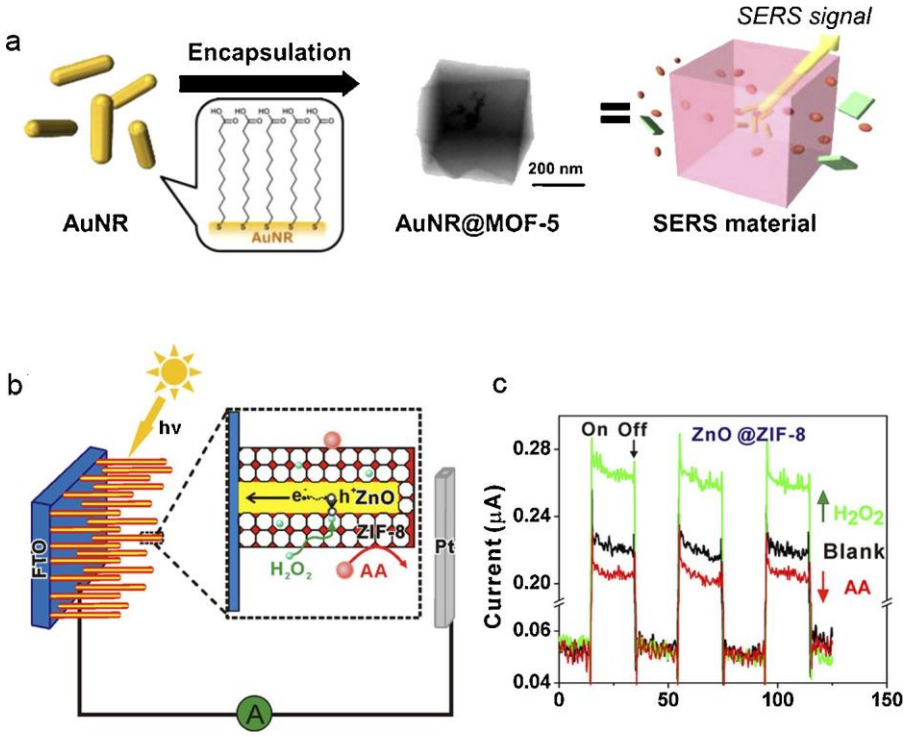

Fig. 9. (a) Schematic illustration of SERS sensing activity of MOF-5 supported Au nanorods. Reproduced from [10]. (b) Schematic diagram of ZIF-8 supported ZnO nanorods PEC sensors with selectivity to H_2O_2. (c) Photocurrent response of this sensor in the presence of H_2O_2 (0.1 mM) and ascorbic acid (0.1 mM). Reproduced from [137].

occurring when the analytes are adsorbed on metal nanoparticles (e.g. plasmonic Au nanorods) [132-134]. Interestingly, Sada's group showed that the SERS signal enhancement occurred only for certain types of pyridine derivatives, such as pyridine and 2,6-biphenylpyridine, but not for poly(4-vinylpyridine). This selectivity was attributed to the fact that small molecules such as pyridine and 2,6-biphenylpyridine can diffuse into the pores of MOF-5 and reach the embedded Au nanorods. On the contrary, bulky poly(4-vinylpyridine) molecules cannot diffuse into MOF-5 and cannot interact with Au nanorods. Very recently, a similar strategy was used to follow the metalation of a porphyrin-based MOF [135]. In this study, SERS-active Ag nanoparticles were wrapped with crystals of this MOF.

Other size-selective sensors composed of MOFs and metal nanoparticles have been reported. These system were used to monitor electrochemical changes of Pt nanoparticles [136], photoelectrochemical changes of ZnO nanorods [137] and luminescence changes of CdSe quantum dots. Xu et al. showed the possibility to selectively detect H_2O_2 using UiO-66 supported Pt nanoparticles [136]. One of the main concerns for a H_2O_2 electrochemical sensor is the presence of other physiological species such as ascorbic acid, uric acid and some carbohydrate compounds, which can be also oxidized along with H_2O_2 molecules on the electrode surface and cause interference. This issue was solved by embedding the Pt nanoparticles into UiO-66, which acts as a size-exclusion filter allowing only H_2O_2 molecules to diffuse in, while excluding the bulkier interfering ascorbic acid, uric acid, and carbohydrate compounds. Selective photoelectrical detection of H_2O_2 was demonstrated using a similar approach, by coating ZnO nanorods with ZIF-8 (Fig. 9b) [137]. Here, the ZIF-8 network also acts as a size-exclusion filter preventing the diffusion of ascorbic acid molecules while allowing diffusion of the smaller H_2O_2 molecules to the ZnO nanorods. Illuminating the sample with 380 nm light engendered a photocurrent response that arises from the oxidation of H_2O_2 by photogenerated holes on the surface of ZnO nanorods (Fig. 9c). Finally, Falcaro and co-workers demonstrated the size selective detection of ethanethiol compared to a larger linear copolymer n-isopropyl acrylamide/acrylic acid/t-butyl acrylamide mercaptane, by following the quenching effect of luminescent CdSe quantum dots embedded into MOF-5 [9,138]. The same group grew MOF-5 around Co NPs and subsequent infiltration with a dye enabled the fabrication of a repositionable sensor for the detection of aromatic amines [139].

4.2. Gas selective-sensors

In addition to size selective sensors, the potential of MOFs to tune the chemical functionality of their pores for the selective adsorption of certain species also paves new ways to create chemically selective sensors when combined with responsive metal nanoparticles. For example, it is well-known that MOF-5 is selective towards CO_2 in a gas mixture because the polarizability and quadrupole moment of CO_2 leads to electrostatic attraction between CO_2 molecules and the aromatic rings of MOF-5 [140]. Using this property, Tang's group synthesized a Au@MOF-5 SERS sensor able to selectively detect CO_2 in the presence of various gases [141].

4.3. Ion-selective sensors

Recent advances have led to selective sensors based on other mechanisms; e.g., taking advantage of the low chemical stability of some MOFs. Using this approach, Zhao et al. developed a sensor selective for phosphate ions by embedding ZnO quantum dots into MOF-5 [142]. The working mechanism of this sensor was simple: MOF-5 degrades in the presence of phosphate ions, thus liberating the ZnO nanoparticles, that recover their original fluorescence that was quenched when embedded. The authors showed the selectivity of this sensor for phosphates by exposing it to various other anions, resulting in a much lower fluorescence signal.

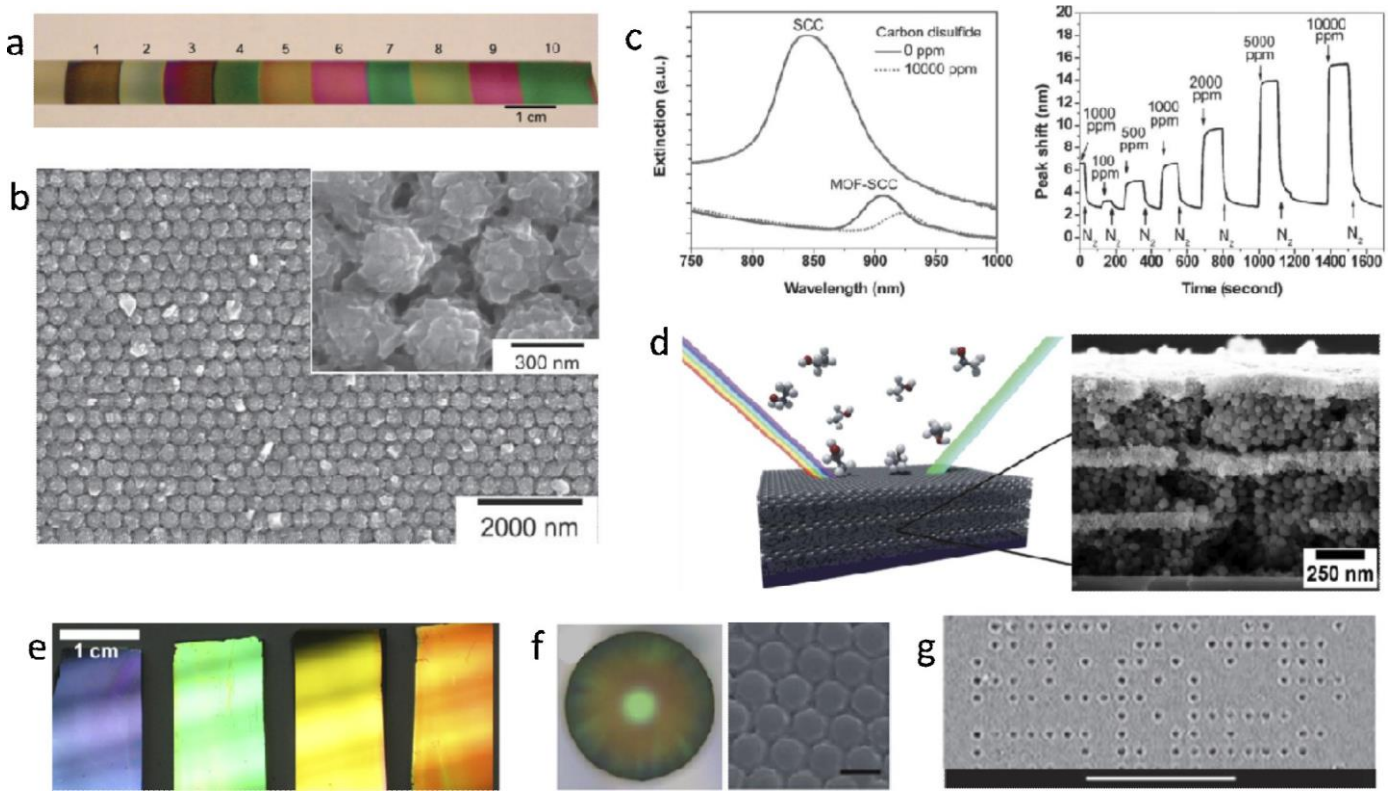

Fig. 10. MOF-based photonic crystals for label-free optical sensing. (a) Photograph of a series of ZIF-8 films of various thicknesses grown on silicon substrates. Reproduced from [143]. (b) SEM images of the MOF-silica photonic crystals prepared by step-by-step deposition of HKUST-1. Inset: high magnification. (c) Left: Near-IR extinction spectra of the MOF-silica photonic crystal (MOF-SCC) and the bare silica colloidal (SCC) crystal film before and after exposure to 10 000 ppm CS_2 . Right: Response of MOF-silica photonic crystal to a series of CS_2 vapors of various concentrations versus time. Reproduced from [146]. (d) Left: Schematic representation of a Bragg stack. Right: SEM images of a Bragg stack prepared by alternatingly spin-coating nanoparticulate suspensions of ZIF-8 and TiO_2 , resulting in a layer thickness of approx. 200 nm and 50 nm for ZIF-8 and TiO_2 , respectively. Reproduced from [152]. (e) Photographs of step-by-step HKUST-1/ITO hybrid materials with different thickness. The stripes are caused by the light source. Reproduced from [156]. (f) Left: Optical image of a MOF-5/silica composite sphere with a diameter of 200 m. Right: Corresponding SEM image showing the uniform silica spheres with interstitial MOF-5. Scale bar: 300 nm. Reproduced from [157]. (g) Transmission optical microscopy image of a metallic silver dot pattern deposited inside a single MOF-5 crystal. Scale bar: Scale bar: 25 m. Reproduced from [148].

4.4. Photonic crystal sensors

Color change is another attractive sensing mechanism, as it can be readily detected, in some cases even with the naked eye. Solvatochromism/vapochromism and luminescence color or intensity shifts have been reported for MOFs upon guest accomodation [129]. However, such behavior is based on specific responsive elements in the lattice that might not be compatible with fine-tuning the adsorption properties to detect different analytes. Therefore, a more flexible approach would require fine-tuning the MOF adsorption behavior without having to take the preservation of color change capabilities into account. In this context, Lu et al. demonstrated sensing based on the color change of the light reflecting off of a thin ZIF-8 film on a flat surface (Fig. 10a) [143]. The underlying principle is Fabry-Pérot interference, which occurs when incident light undergoes multiple reflections off of two parallel surfaces separated by a distance on the order of the wavelength of light. The wavelengths at which constructive interference occurs, which determines the color of the reflected light, depends on the refractive index of the film. Since the refractive index of a microporous material increases when guests are accommodated in the pores, the concentration of propane in N_2 correlates with the interference peak shifts.

The performance of interference-based sensors can be improved by alternating high- and low-refractive index materials. Label-free optical sensors of this type are referred to as ‘photonic crystals’ [144]. Metal and metal oxide nanoparticles composite can be used as effective materials for sensing applications due to the difference between the refractive index of the MOF and the encapsulated inorganic nanoparticles. Lu et al. first illustrated this depositing a conformal HKUST-1 coating on an array of uniform carboxylic acid terminated silica spheres, using a step-by-step protocol (Fig. 10b) [145,146]. When exposed to carbon disulphide (CS_2) vapors, the wavelength of the light reflecting off of the photonic crystal shifted gradually with increasing CS_2 concentrations while a bare silica colloidal crystal did not generate a response (Fig. 10c). Similar three-dimensional photonic crystals can also be fabricated using regular assemblies of uniform polymer beads instead of silica spheres [147]. Infiltration of such polymer colloidal crystal templates with MOF precursor solutions [148] and subsequent dissolution of the polymer template results in photonic crystals where the alteration of high- and low-refractive index components is ensured by the continuous MOF structure and regularly spaced air gaps therein, respectively [149,150]. Similar behavior is observed in stacked layers of well-formed and uniform MOF crystallites [151].

Another approach for the fabrication of photonic MOF-based sensors, requires alternating layers of high- and low-refractive index materials stacked on top of each other, to yield one-dimensional photonic crystals or Bragg stacks. Although these are not discrete nanoparticles imbedded within MOF crystals, but rather superstructures that requires both nanoparticle and MOF components localized in different layers, we will briefly discuss such composites to highlight this emerging application. The Bragg stack reflectivity can be enhanced by increasing the number of layers, or by the judicious choice of materials to increase the refractive index contrast. Hinterholzinger et al. demonstrated Bragg stacks

based on ZIF-8 and high-refractive index TiO_2 [152]. Two fabrication methods were employed: (1) alternating spin-coating of nanoparticulate suspensions of both materials and (2) alternating ZIF-8 growth and spin-coating of TiO_2 particles. While the former technique yields a high degree of textural mesoporosity in both layer types, in addition to the ZIF-8 microporosity, the latter method results in Bragg stacks featuring continuous ZIF-8 layers (Fig. 10d). Alcohols too large to efficiently enter the ZIF-8 pores triggered small and large responses in the sensors obtained with method 1 and 2, respectively. These tests indicate that to enable molecular sieving in a photonic crystal, continuous MOF films are perferred. Nevertheless, the particle spin-coating method remains popular, mainly because of its simplicity and general applicability [153,154]. For instance, Hu et al. demonstrated how Bragg stacks of the flexible MIL-88B-NH_2 and TiO_2 can be used for the determination of the EtOH content of aqueous solutions of the alcohol [153]. Ranft et al. showed how the response from three spin-coated MOF-TiO_2 Bragg stacks with different adsorption preferences could be combined to generate a unique signature for each analyte and thus enhance specificity in comparison to that of the individual sensors [154].

The deposition of both the MOF layer and high-refractive index component as continuous films provides the highest reflectivity MOF-based Bragg stacks. Thus far only two cases of monolithic MOF-based Bragg stacks have been demonstrated. Lu et al. showed how metal sputtering in combination with the ZIF-8 film growth method led to one-dimensional photonic crystals [146,155]. The Bragg stack with the highest reflectivity reported to date (ca. 80%) was created by Liu et al. by alternating the sputtering of indium tin oxide (ITO) and the deposition of HKUST-1 layers via the step-by-step protocol (Fig. 10e) [156].

One potential issue with the practical implementation of photonic crystals is the angle-dependency of the observed color [155]. Cui et al. proposed an interesting approach to fabricate color shift sensors exhibiting full angle independence that work similarly to the three-dimensional photonic crystals discussed above [157] (Fig. 10f).

Another exciting development is the demonstration by Ameloot et al. of depositing metallic microstructures within single crystals of a photoactive MOF material in a programmed fashion [148]. This method enables the fabrication of three-dimensional metal dot arrays arranged in an arbitrary pattern within a MOF crystal (Fig. 10g), thus resulting in a regular arrangement of high- and low-refractive index materials. Since the generation of such arrays is fully computer-controlled, fine-tuning the optical response for photonic sensing applications should be straightforward.

5. NP@MOFs for sequestration and separation

The high and tunable porosity of MOFs eases the penetration, accumulation, and separation of various species not only from gas but also from liquid phase. Nanoparticles embedded inside MOF structures can impart additional functionalities. For example, enabling the recollection using a magnetic field of the MOF used as a sorbent for pollutants, using the photocatalytic properties for their degradation, or acting a support that facilitate the separation of organic compounds (Fig. 11).

5.1. Sequestration of pollutants

MOFs have shown great potential for the removal of carcinogenic polycyclic aromatic hydrocarbons (PAHs), heavy metals, pesticides, dyes, radionucludes and other toxic chemicals [158-164]. Introducing additional functionality via magnetic nanoparticles can be achieved by synthesizing magnetic framework

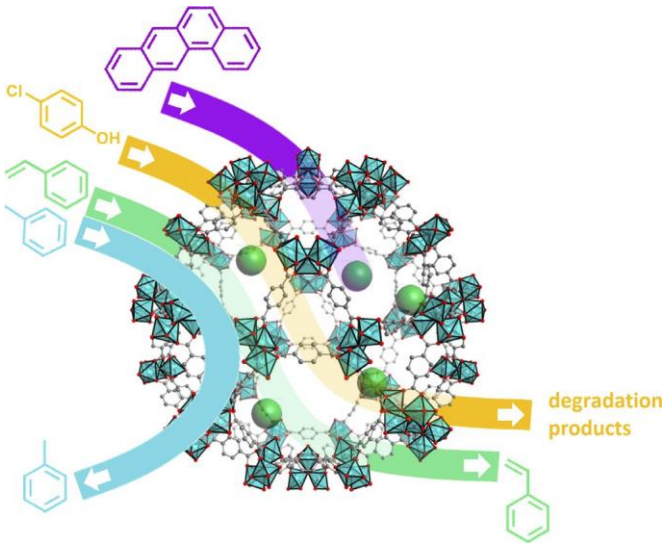

Fig. 11. Schematic illustration of metal/metaloxide nanoparticles@MOF for pollutant sequestrations and degradation, and separation.

composites (MFCs) [165]. There are two main advantages provided by the magnetic particles. Firstly, they facilitate positioning the porous material using an external magnetic force. This can have application to simple magnetic recovery in a batch reactor to more precise localization in microfluidic devices. Secondly, magnetic nanoparticles afford a magneto-thermal effect when exposed to an alternate magnetic field which can be exploited to release guests from the pores of the MFCs [166]. We note that the surface area of the MFCs are lower compared to the parent MOF due to the gravimetric contribution of the particles that, under optimized conditions, lies in the range of 3-5 wt% (e.g. 4% using Co nanoparticles [139]).

The use of MFCs for the sequestration of polycyclic aromatic hydrocarbons (PAHs) has been reported by Doherty et al. [167] and Huo and Yan [168] in 2012. Yan demonstrated that silica coated magnetic iron oxide and MIL-101(Cr) could be mixed and used for the efficient recovery (81-96%) of six different PAHs from water, while Doherty et al. showed that cobalt and nickel ferrites superparamagnetic nanofibers directly embedded into MOF-5 crystals afforded a 1.3 mmol g^{-1} uptake of benz[a]anthracene (Fig. 12a). In 2013, the group of Maspoch [169] synthesized iron oxide embedded in the copper based MOF HKUST-1 using a spray-drying method. The resulting spherical magnetic framework composite was used for capturing dibenzothiophene (DBT) from iso-octane with a remarkable extraction capacity of 200 g kg^{-1} (Fig. 12b). Chen and co-workers [72] investigated using core-shell magnetic spheres, made with a magnetic iron oxide core and a MIL-100(Fe) MOF shell, towards the sequestration of polychlorinated biphenyls (PCBs) from water. This MOF composite yielded excellent recovery (above 81%) of the PCB, and it was also being able to reach a very low limit of detection (down to 1.07 ng L^{-1}), suitable for harvesting trace amounts of pollutant.

A second important application in environmental remediation is related to inorganic pollutants, such as heavy metals [170,171]. This is due to the environmental and health issues connected with the contamination from, particularly Pb, Hg, Ni, Cr, and Cd. Additionally, the efficient sequestration of certain rare heavy metals such as Ag, Au, Pd, and Pt is of interest because of their high economic value. Examples of MFCs exploited for the collection of dangerous heavy metals have been reported by Sohrabi et al. [172], Wang et al. [173], and Taghizadeh et al. [174]. All these studies used modified silica-coated, iron oxide nanoparticles embedded into HKUST-1. Sohrabi

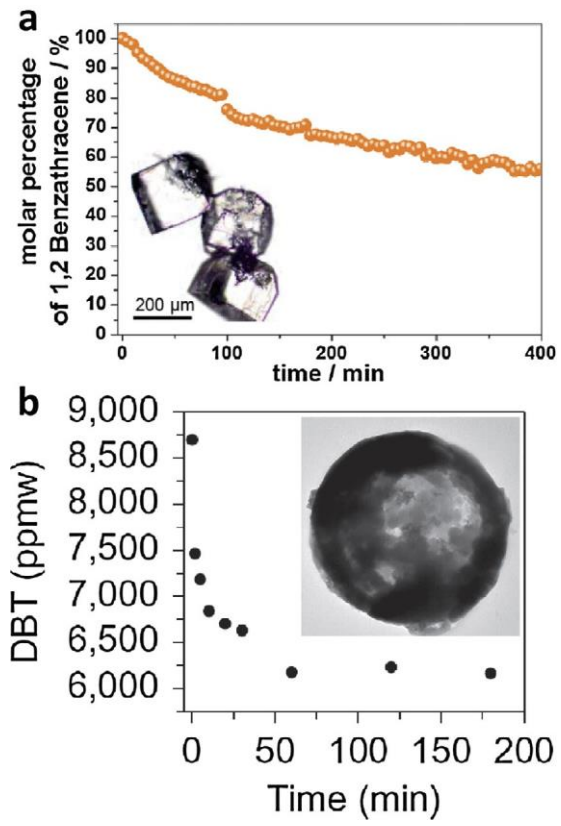

Fig. 12. (a) Change in molar percentage of benz[a]anthracene during time due to the uptake performed by $CoFe_2O_4$ @MOF-5 composite (in the inset). Reproduced from [167]; (b) Time dependence of the dibenzothiophene capture by Iron oxide nanoparticle@HKUST-1 superstructure (in the inset) obtained by spray-drying. Reproduced from [169].

explored the optimization of Cd(II) and Pb(II) ions uptake using pyridine grafted on the surface of the magnetic particles. Excellent extraction values of ca.190 mg g^{-1} were reported. Wang et al. chose post-functionalization of magnetite@HKUST-1 with dithizone as a strategy for the sequestration of Pb(II) obtaining a modest uptakes of 1.67 mg g^{-1}. Based on a very similar system to Sohrabi [172], Taghizadeh studied the uptake of Cd(II), Pb(II), Ni(II), and Zn(II), reported sequestration values between 98 (Ni) and 206 (Zn) mg g^{-1}. The capture of high value heavy metals by MFCs has been canvassed in the work of Falcaro et al. [175] and Bagheri et al. [176]. In the first case, a composite based on a MOF made of two linkers (terephthalic acid and 2-aminoterephthalic acid) and Co nanoparticles was used to selectively harvest Ag(I) ions from a microchannel, in which the MFCs were moved from a dodecanol filled zone to a silver enriched methanol one. It was posited that sequestration of Ag(I) ions was due to the presence of the amino groups in the MOF pores. Finally, the nanocomposite was moved to a third channel filled with dodecanol for recovery. In the work of Bagheri et al. [176], the aforementioned pyridine functionalized iron oxide magnetic particles embedded into HKUST-1 were used to collect Pd from water with a maximum absorption capacity of 105 mg g^{-1}.

5.2. Uptake and degradation

A different strategy in environmental remediation is the concomitant removal and degradation of pollutants, particularly with respect to noxious organic agents. In this case, the high uptake capacity afforded by the MOF and the potential of the embedded nanoparticles to decompose pollutant molecules are utilised.

In 2013, Shen et al. [114] proposed a pioneering study that described the simultaneous uptake and degradation of toxic species, such as hexavalent chromium and model dyes, using Pd@NH2-UiO66. In this composite, small Pd nanoparticles (3-6 nm) were homogeneously generated within the pores of a preformed amino functionalized UiO-66 MOF. Under a 420 nm visible light irradiation, this system was able to photo-catalytically reduce the carcinogenic Cr(VI) to Cr(III) within 90 min at a pH range of 1-5, demonstrating superior performance when compared with bare NH_2-UiO66 and N-doped titania. More interestingly, the same system was investigated toward the complete degradation of methyl orange (MO) and methylene blue (MB). Here, the measured conversion was modest when using either the dye (5% for MO and 38% for MB) or the Cr(VI) alone. However, this conversion drastically enhanced when the dye was added to the reaction system: Cr(VI) reduction increased from initial 70% to 79% in presence of MO, and from 70% to nearly 100% in presence of MB, demonstrating a beneficial synergistic effect.

Among the different active materials with degradation capabilities, titania particles are extensively used as efficient photocatalytic nanomaterials, especially for self-cleaning surfaces [177,178]. For such purpose, Hu and co-workers [179] studied the TiO_2@MIL-101(Cr) composite, which was prepared by post-infiltration of different amounts of tert-butyl titanate into the MOF cavities. The resulting titania was then converted to the more photocatalyticaly active anatase phase by thermal treatment. The composite demonstrated higher adsorption of formaldehyde than the titania alone due to the high surface area of MIL-101(Cr). Additionally, the titania was able to degrade the pollutant using a 100 W lamp at 365 nm. The composite with 14.5 wt% TiO_2 was found to be the most efficient with ca. 80% of product destroyed within 200 min. Furthermore, the same material was successfully used for the degradation of o-xylene with analogous results.

A recent example of one-pot uptake and degradation carried out by a NP@MOF composite was reported by Cai's group [180]. In this work, Fe-doped MOF-5 was prepared around pre-synthesized 60 nm Co_3O_4 nanoparticles, using $Fe(acac)_3$ as the source of iron (Fig. 13a) [181]. The high porosity and open pore network of the MOF structure enables fast molecule diffusion, thus rapidly concentrating the pollutant species (in this case, 4-chlorophenol) and exposing it to the catalytic nanoparticles for its degradation. In this case, the degradation was mediated by potassium peroxymonosulfate (Oxone), which was diffused into the MOF pores. The as-prepared yolk-shell catalyst was highly active with a removal efficiency of 4-chlorophenol over 99% within 150 min even after four successive cycles (Fig. 13b).

5.3. Stationary phases for separations

Due to their crystalline structure and high porosity, MOFs have recently emerged as candidates for analytical and chromatographic separations [182]. Separation by adsorption is more energy efficient than distillation, but to date limited examples with acceptable selectivity have been reported [183]. Silica is the most common stationary phase used in normal phase chromatography and therefore, a natural step forward is to combine silica and MOFs to achieve better performances. Bradshaw's group [8] introduced a sphere-on-sphere (SOS) technique to immobilize small engineered 200 nm silica nanospheres on 5.5 m silica microspheres. The SOS system with carboxylic groups acted as scaffold for the subsequent growth of HKUST-1 crystals, and the obtained SOS-COOH@HKUST-1 composite (Fig. 14a and b) was packed in a high-performance liquid chromatography (HPLC) column. The results indicated that the composite was able to separate a mixture of toluene, ethylbenzene and styrene using heptanes/dichloromethane 95:5, whereas the neat SOS-COOH showed no separation properties (Fig. 14c and

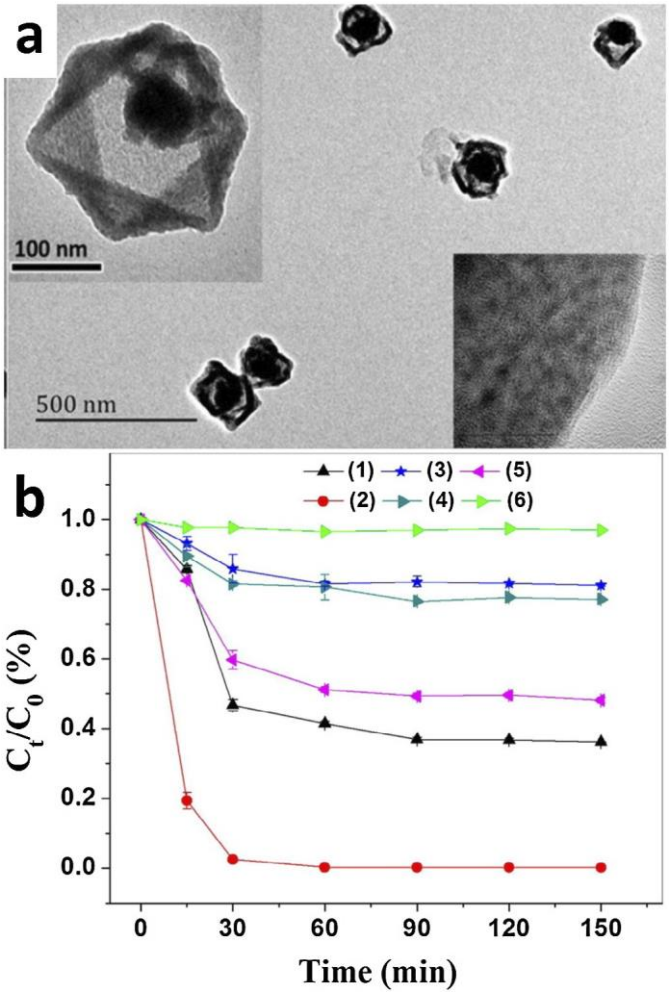

Fig. 13. (a) TEM image of yolk-shell Co3O4@Fe-MOF-5. The insets are closer observations of the composite; (b) Removal of 4-chlorophenol within 2.5 h for bare NPs activated with Oxone (1), yolk-shell composite activated with Oxone (2), composite alone (3), hollow MOF with Oxone (4), solid core-shell composite with Oxone (5), and Oxone only.

Reproduced from ref. [180].

d). Moreover, the same composite was used, after dichloromethane or toluene pre-conditioning for 24 h, to successfully separate xylene isomers using heptane as the mobile phase. Silvestre et al. [184] used layer-by-layer epitaxy to grow HKUST-1 on magnetic silica nanocubes, producing a magnetic framework composite with high surface area (1150 $m^2\ g^{-1}$) after 200 coating cycles. The obtained material was used for HPLC chromatography, showing an appreciable, although incomplete separation of toluene and pyridine. In both cases, the presence of MOFs was found important to enhance, and in some case achieve optimal separation performance.

6. NP@MOFs for controlled release

Molecular delivery is an application of current interest in MOF chemistry [185,186]. In contrast to gas storage and separation, where the focus is to optimise the attractive forces between the framework and guest, the possibility to control the molecular delivery of guests represents an additional challenge. The majority of studies in this area describe the spontaneous release of molecules from the pores [187-190]. This process is driven by the molecular diffusion where, ultimately, the concentration of guest molecules in the pores and external environment reaches equilibrium. This strategy is most suitable for long-term drug release. However, if the release of guests can be triggered by an external stimulus (Fig. 15), further opportunities would arise in more complex systems in cell biology or biomedicine. MOF composites seem to be an effective platform for controlled drug release. Three strategies for triggered release of molecules have been explored using MOF composites: (1) Introduction of photo-switchable molecules into the pore networks that gives rise to guest release upon irradiation [191,192]; (2) Immobilization of target molecules into pore surfaces via photo-labile moieties that undergo controlled photolysis and release of the entrapped molecules [193,194]. We noted that both of these strategies require the specific chemical modifications to the pores' surface; and (3) Exploitation of metal/metal oxide nanoparticles@MOFs nanoparticles where external stimuli, such as a magnetic field or light, causes release of molecules by localized heating. The advantage of this approach relies on the wide variety of frameworks of different pore size and chemistry that can be used to prepare these metal/metal oxide nanoparticles@MOF composites.

Incorporating magnetic metal nanoparticles into MOFs is an example of a metal/metal oxide nanoparticles@MOF composite designed for controlled molecular release [165]. In addition to providing a mechanism for localised heating, the magnetic nanoparticle facilitates spatial control of the composite via the external magnetic field. To this end, Qiu and co-workers have reported the synthesis of Fe_3O_4@HKUST-1 nanocomposites loaded with nimesulide (NIM), a potential anticancer drug for pancreatic cancer treatment (Fig. 16a and b) [195]. This MOF composite maintained its magnetic characteristics at 300 K, thus demonstrating its potential for use in biological systems. Furthermore, these nanoscomposites could be positioned using a magnet in aqueous solution as shown in Fig. 16c. The spontaneous release of NIM over 11 days was examined in physiological saline (aqueous NaCl solution) at 37°C (Fig. 16d); however, controlled release of the drug via an alternating magnetic field was not demonstrated. We note that HKUST-1 is known to be water sensitive [196], hence the spontaneous release of NIM may be attributed to the decomposition of HKUST-1.

A similar study was also reported by Li and co-workers using -Fe_2O_3@MIL-53(Al). In this case, the measured residual magnetization of -Fe_2O_3@MIL-53(Al) indicated that the -Fe_2O_3 nanoparticles were superparamagnetic [197]. Here the spontaneous release of ibuprofen as a model drug over 7 days was reported. However, the stability of this composite in physiological saline solution was not assessed. Given the higher stability of MIL-53(Al) in water [198] than in phosphate buffer saline, it can be expected that the spontaneous release of the drug was regulated by pore diffusion. Kaskel and co-workers further exploited the properties of magnetic nanoparticles into MOFs by triggering the release of molecules via induced magnetic heating (Fig. 17) [166]. In this experiment, -Fe_2O_3@HKUST-1 was suspended in ethanol and, under a magnetic field strength of 1.7 kA m^{-1} at a frequency of 183 kHz, a temperature increase from 23°C to 40°C was measured in less than 10 minutes. A specific absorption rate (SAR) for ibuprofen was determined to be 11.1 W g^{-1}. Because -Fe_2O_3@HKUST-1 showed temperature dependent release kinetics of ibuprofen (passing from 4.4×10^{-6} mmol s^{-1} at 20°C to 6.6×10^{-6} mmol s^{-1} at 40°C), the high SAR value will effectively contribute to the release of drugs induced by an external magnetic field. Accordingly, real-time monitoring of drug release under an external magnetic field should be investigated to fully evaluate the potential of this system.

Gold nanorods (GNRs) are known to generate heat by absorption of near infrared light, the so-called photothermal conversion effect [199]. Furukawa and co-workers demonstrated the synthesis of core-shell type mesoscopic composites of GNR@[Al(OH)(1,4-ndc)]$_n$ from GNR@alumina via coordination replication (Fig. 18)

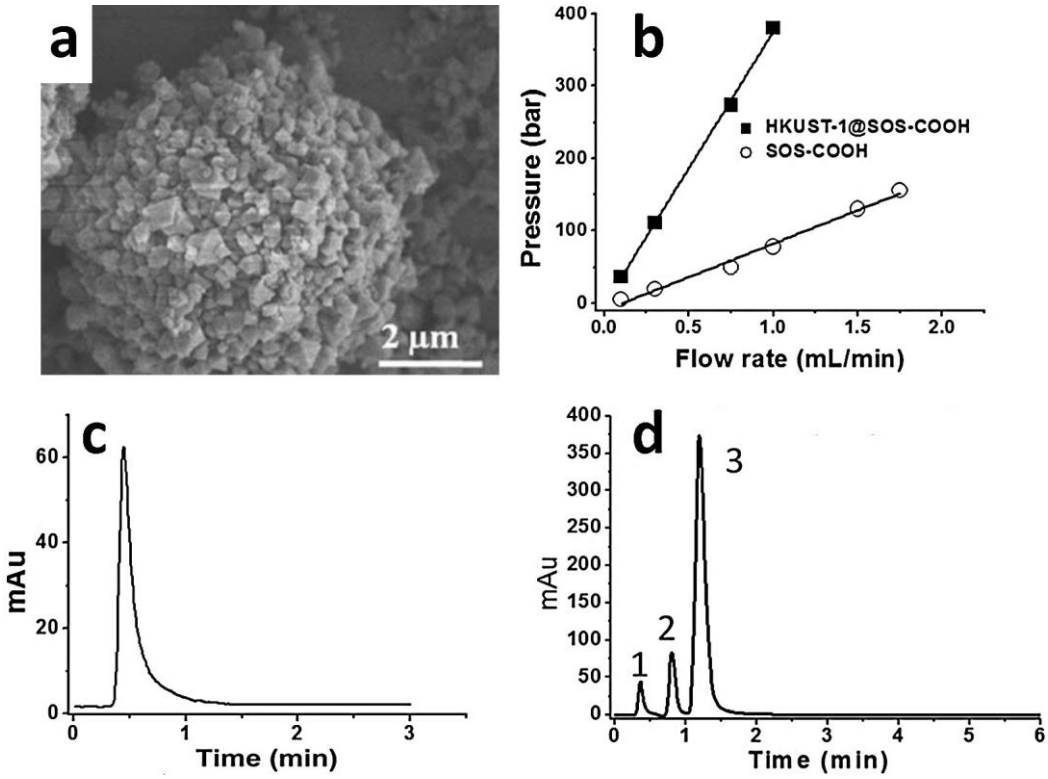

Fig. 14. (a) SEM of SOS-COOH@HKUST-1 particles; (b) back-pressure vs flow rate measured for columns packed with SOS-COOH particles (empty circles) and SOS-COOH@HKUST-1 particles (black squares) using heptanes as mobile phase; (b) chromatogram showing that column packed with SOS-COOH particles was not able to separate a mixture of ethylbenzene and styrene; (c) chromatogram obtained using column packed SOS-COOH@HKUST-1 particle in heptane/DCM 95:5 as mobile phase, for the separation of toluene (1), ethylbenzene (2), and styrene (3).

Reproduced from ref. [8].

[13]. In this case, anthracene was selected as the model guest specie as it can be easily monitored by fluorescence spectroscopy. Interestingly, spontaneous release (i.e. leakage) of anthracene from the pores was not observed in cyclohexane. However, molecular release was confirmed under near infrared light (750 nm) irradiation. Most of molecules (ca. 70%) were released from the pores of $[Al(OH)(1,4\text{-ndc})]_n$ in 2 h. This work represents the highest level of control achieved for the triggered release of molecules from metal nanoparticles@MOFs.

As shown here, the hybridization of MOFs with metal nanoparticles is a promising strategy for inducing molecular release via a non-destructive external stimulus (magnetic field, near IR light). However, there are still very few examples of metal nanoparticles @MOFs for delivery applications and further proof-of-concept model systems will be essential to a comprehensive understanding of their chemistry and potential for real biological application. The key elements that need to be addressed are the following: (1) careful experimental design that directly monitors molecular release under external stimuli; (2) development of physiologically stable non-toxic MOFs; and (3) understanding the host-guest interactions between the MOFs and selected drugs, so that controlled release can be realised without drug leakage.

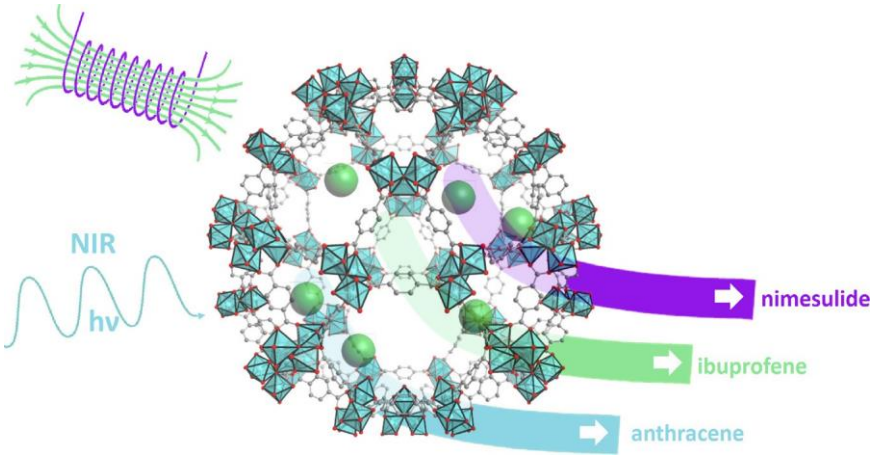

Fig. 15. Schematic illustration of controlled molecular release from metal/metal oxide nanoparticles@MOF. Thanks to the capability of magnetic iron oxide nanoparticles or gold nanorods, which convert magnetic field or near IR into heat, respectively, the release of trapped molecules can be initiated by physical stimuli.

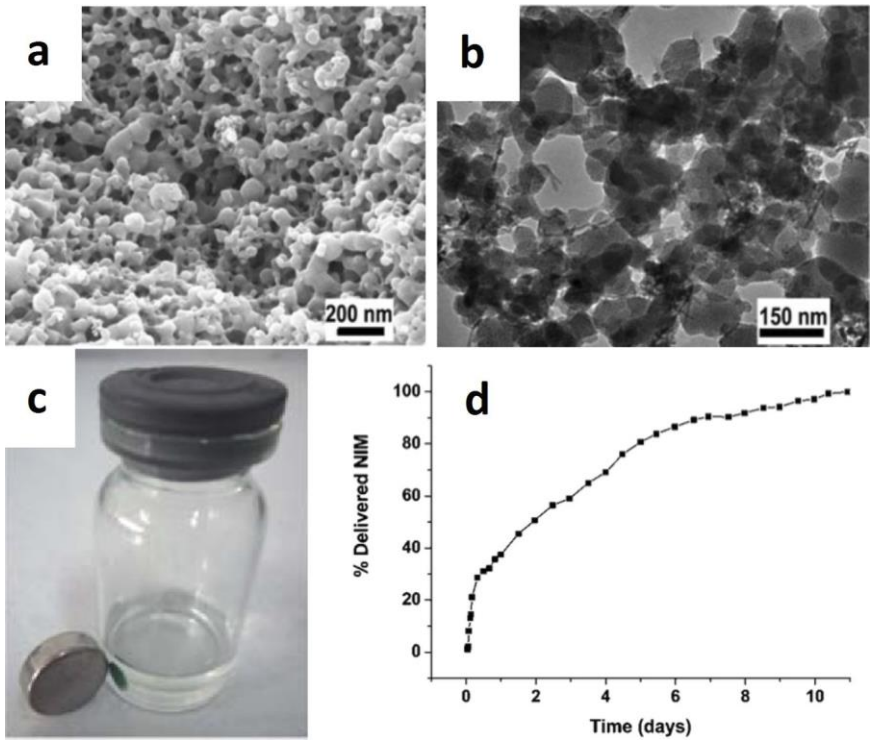

Fig. 16. (a) SEM and (b) TEM images of Fe_3O_4 @HKUST-1 composites. (c) NIM loaded Fe_3O_4 @HKUST-1 composites attracted by a magnet. (d) Spontaneous release of NIM from Fe_3O_4 @HKUST-1 in physiological saline solution at 37° C.
Reproduced from ref. [195].

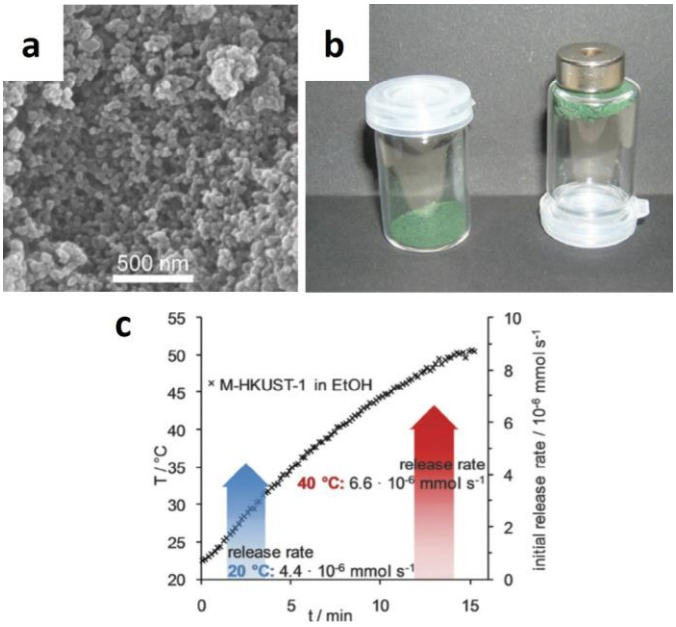

Fig. 17. (a) SEM image of g-Fe_2O_3 @HKUST-1 composites. (b) Fe3O4@HKUST-1 composites attracted by a magnet. (c) Magnetic heating curve of 324 mg of g-Fe_2O_3 @HKUST-1 composites in 30 mL of ethanol at 183 kHz and a field strength of 1.7 kA m^{-1} . The arrows indicate the initial release rates for ibuprofen at 20 and 40° C, respectively.
Reproduced from ref. [166].

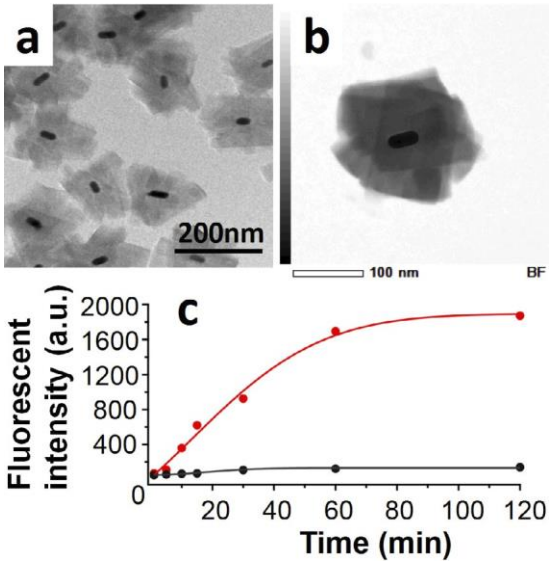

Fig. 18. (a and b) TEM image of GNR@[Al(OH)(1,4-ndc)]n composites. (c) Evaluation of anthracene release from GNR@[Al(OH)(1,4-ndc)]n composites. The graph shows liner plots for fluorescence intensity maxima of the released anthracene versus time with (red) and without (black) light irradiation at 750 nm.
Reproduced from ref. [13].

7. Future outlook

In this review we have shown how nanocomposites obtained by the judicious combination of metal/metal oxide nanoparticles with MOFs can be used as advanced materials for wide variety of applications including gas adsorption, separation, catalysts, molecular sieve and repositionable sensors, environmental remediation, and drug-delivery. Importantly, these nanocomposites are now being explored for more sophisticated and emerging technologies such as microfluidics where the nanocomposites can be used as micro-carriers [175], photocatalysts for H_2 production [200], or biomedical applications where 'up-conversion' properties can facilitate photoregulated drug release [201].

Despite the amount of studies proposed in the literature, we posit that we are at the early stage of this emerging research field. We base this notion on the following: (1) the potential for integrating sophisticated inorganic nano-systems with a variety of properties including plasmonic, electro- and thermo-chromic, up- and down-conversion properties into the composites; (2) the ever and increasing number of MOFs possessing customized chemical functionalities and tailored pore size and arrangement; (3) the rapid progress in the preparation methods for nanoparticles and MOFs that will further facilitate their integration; and (4) the potential to engineer multicomponent nanocomposite systems that can incorporate multiple nanoparticles within different MOFs systems. Finally, in order to fully realize the potential of this area, a fundamental understanding of the mechanisms that imbue the composites with their unique properties (e.g. spill over effect, heat transfer mechanisms, and energy gap modulation) must be pursued. This will help to build a solid platform towards the engineering of these exciting and novel materials for practical applications.

Acknowledgements

P.F. and C.J.D. gratefully acknowledges the Australian Research Council for funding DECRA DE120102451 and Future Fellowships FT100100400, respectively. D.M., I.I. and A.Y. thank the EC FP7 ERC-Co 61594.

References

[1] H. Deng, C.J. Doonan, H. Furukawa, R.B. Ferreira, J. Towne, C.B. Knobler, B. Wang, O.M. Yaghi, Science 327 (2010) 846.
[2] S. Kitagawa, R. Kitaura, S. Noro, Angew. Chem. Int. Ed. 43 (2004) 2334. [3] H. Furukawa, K.E. Cordova, M. O'Keeffe, O.M. Yaghi, Science 341 (2013) 974. [4] M. O'Keeffe, O.M. Yaghi, Chem. Rev. 112 (2012) 675.
[5] V. Guillerm, D. Kim, J.F. Eubank, R. Luebke, X. Liu, K. Adil, M.S. Lah, M. Eddaoudi, Chem. Soc. Rev. 43 (2014) 6141.
[6] Q.-L. Zhu, Q. Xu, Chem. Soc. Rev. 43 (2014) 5468.
[7] G. Lu, S. Li, Z. Guo, O.K. Farha, B.G. Hauser, X. Qi, Y. Wang, X. Wang, S. Han, X. Liu, J.S. DuChene, H. Zhang, Q. Zhang, X. Chen, J. Ma, S.C.J. Loo, W.D. Wei, Y. Yang, J.T. Hupp, F. Huo, Nat. Chem. 4 (2012) 310.
[8] A. Ahmed, M. Forster, R. Clowes, D. Bradshaw, P. Myers, H. Zhang, J. Mater. Chem. A 1 (2013) 3276.
[9] P. Falcaro, A.J. Hill, K.M. Nairn, J. Jasieniak, J.I. Mardel, T.J. Bastow, S.C. Mayo, M. Gimona, D. Gomez, H.J. Whitfield, R. Riccò, A. Patelli, B. Marmiroli, H. Amenitsch, T. Colson, L. Villanova, D. Buso, Nat. Commun. 2 (2011) 237.
[10] K. Sugikawa, S. Nagata, Y. Furukawa, K. Kokado, K. Sada, Chem. Mater. 25 (2013) 2565.
[11] G. Li, H. Kobayashi, J.M. Taylor, R. Ikeda, Y. Kubota, K. Kato, M. Takata, T. Yamamoto, S. Toh, S. Matsumura, H. Kitagawa, Nat. Mater. 13 (2014) 802.
[12] R. Ameloot, F. Vermoortele, W. Vanhove, M.B.J. Roeffaers, B.F. Sels, D.E. De Vos, Nat. Chem. 3 (2011) 382.
[13] K. Khaletskaya, J. Reboul, M. Meilikhov, M. Nakahama, S. Diring, M. Tsujimoto, S. Isoda, F. Kim, K. Kamei, R.A. Fischer, S. Kitagawa, S. Furukawa, J. Am. Chem. Soc. 135 (2013) 10998.
[14] K. Liang, R. Ricco, C.M. Doherty, M.J. Styles, S. Bell, N. Kirby, S. Mudie, D. Haylock, A.J. Hill, C.J. Doonan, P. Falcaro, Nat. Commun. 6 (2015) 7240.
[15] J.D. Evans, C.J. Sumby, C.J. Doonan, Chem. Soc. Rev. 43 (2014) 5933.
[16] C. Rösler, R.A. Fischer, CrystEngComm 17 (2015) 199.
[17] S. Hermes, F. Schr?der, S. Amirjalayer, R. Schmid, R.A. Fischer, J. Mater. Chem. 16 (2006) 2464.
[18] C. Zlotea, R. Campesi, F. Cuevas, E. Leroy, P. Dibandjo, C. Volkringer, T. Loiseau, G. Férey, M. Latroche, J. Am. Chem. Soc. 132 (2010) 2991.
[19] M. Saikia, D. Bhuyan, L. Saikia, New J. Chem. 39 (2015) 64.
[20] R.J.T. Houk, B.W. Jacobs, F.E. Gabaly, N.N. Chang, A.A. Talin, D.D. Graham, S.D. House, I.M. Robertson, M.D. Allendorf, Nano Lett. 9 (2009) 3413.
[21] L. He, L.F. Dumée, D. Liu, L. Velleman, F. She, C. Banos, J.B. Davies, L. Kong, RSC Adv. 5 (2015) 10707.
[22] C.M. Doherty, D. Buso, A.J. Hill, S. Furukawa, S. Kitagawa, P. Falcaro, Acc. Chem. Res. 47 (2014) 396.
[23] J. Reboul, S. Furukawa, N. Horike, M. Tsotsalas, K. Hirai, H. Uehara, M. Kondo, N. Louvain, O. Sakata, S. Kitagawa, Nat. Mater. 11 (2012) 717.
[24] J.L.C. Rowsell, O.M. Yaghi, Angew. Chem. Int. Ed. 44 (2005) 4670.
[25] K. Sumida, D.L. Rogow, J.A. Mason, T.M. McDonald, E.D. Bloch, Z.R. Herm, T.-H. Bae, J.R. Long, Chem. Rev. 112 (2012) 724.
[26] T. Düren, L. Sarkisov, O.M. Yaghi, R.Q. Snurr, Langmuir 20 (2004) 2683.
[27] M. Eddaoudi, J. Kim, N. Rosi, D. Vodak, J. Wachter, M. O'Keeffe, O.M. Yaghi, Science 295 (2002) 469.
[28] M. Yamauchi, H. Kobayashi, H. Kitagawa, ChemPhysChem 10 (2009) 2566.
[29] Y. Li, R.T. Yang, J. Am. Chem. Soc. 128 (2006) 726.
[30] R. Prins, Chem. Rev. 112 (2012) 2714.
[31] N.R. Stuckert, L. Wang, R.T. Yang, Langmuir 26 (2010) 11963.
[32] Y. Li, R.T. Yang, J. Am. Chem. Soc. 128 (2006) 8136.
[33] Y.-Y. Liu, J.-L. Zeng, J. Zhang, F. Xu, L.-X. Sun, Int. J. Hydrog. Energy 32 (2007) 4005.
[34] X.M. Liu, S. Rather, Q. Li, A. Lueking, Y. Zhao, J. Li, J. Phys. Chem. C 116 (2012) 3477.
[35] C.-S. Tsao, M.-S. Yu, C.-Y. Wang, P.-Y. Liao, H.-L. Chen, U.-S. Jeng, Y.-R. Tzeng, T.-Y. Chung, H.-C. Wu, J. Am. Chem. Soc. 131 (2009) 1404.
[36] Y. Li, F.H. Yang, R.T. Yang, J. Phys. Chem. C 111 (2007) 3405.
[37] A. Mavrandonakis, W. Klopper, J. Phys. Chem. C 112 (2008) 3152.
[38] Y. Li, F.H. Yang, R.T. Yang, J. Phys. Chem. C 112 (2008) 3155.
[39] K. Lee, Y.-H. Kim, Y.Y. Sun, D. West, Y. Zhao, Z. Chen, S.B. Zhang, Phys. Rev. Lett. 104 (2010) 236101.
[40] S.M. Luzan, A.V. Talyzin, Microporous Mesoporous Mater. 135 (2010) 201.
[41] M. Hirscher, Microporous Mesoporous Mater. 135 (2010) 209.
[42] Y. Li, L. Wang, R.T. Yang, Microporous Mesoporous Mater. 135 (2010) 206.
[43] M. Sabo, A. Henschel, H. Fröde, E. Klemm, S. Kaskel, J. Mater. Chem. 17 (2007) 3827.
[44] Y.E. Cheon, M.P. Suh, Angew. Chem. Int. Ed. 48 (2009) 2899.
[45] S. Proch, J. Herrmannsdörfer, R. Kempe, C. Kern, A. Jess, L. Seyfarth, J. Senker, Chem.-Eur. J. 14 (2008) 8204.
[46] D. Banerjee, A.J. Cairns, J. Liu, R.K. Motkuri, S.K. Nune, C.A. Fernandez, R. Krishna, D.M. Strachan, P.K. Thallapally, Acc. Chem. Res. 48 (2015) 211.
[47] R. Grosse, R. Burmeister, B. Boddenberg, A. Gedeon, J. Fraissard, J. Phys. Chem. 95 (1991) 2443.
[48] J. Liu, D.M. Strachan, P.K. Thallapally, Chem. Commun. 50 (2013) 466.
[49] J.A. Kent (Ed.), Kent and Riegel's Handbook of Industrial Chemistry and Biotechnology, Springer US, Boston, MA, 2007.
[50] L. Lloyd, Handbook of Industrial Catalysts, Springer US, Boston, MA, 2011.
[51] R.M. Rioux, H. Song, J.D. Hoefelmeyer, P. Yang, G.A. Somorjai, J. Phys. Chem. B 109 (2005) 2192.
[52] D. Astruc, F. Lu, J.R. Aranzaes, Angew. Chem. Int. Ed. 44 (2005) 7852.
[53] S. Hermes, M.-K. Schröter, R. Schmid, L. Khodeir, M. Muhler, A. Tissler, R.W. Fischer, R.A. Fischer, Angew. Chem. Int. Ed. 44 (2005) 6237.
[54] M. Zhao, K. Deng, L. He, Y. Liu, G. Li, H. Zhao, Z. Tang, J. Am. Chem. Soc. 136 (2014) 1738.
[55] M. Homel, T.M. Gür, J.H. Koh, A.V. Virkar, J. Power Sources 195 (2010) 6367.
[56] H.-L. Jiang, B. Liu, T. Akita, M. Haruta, H. Sakurai, Q. Xu, J. Am. Chem. Soc. 131 (2009) 11302.
[57] E.V. Ramos-Fernandez, C. Pieters, B. van der Linden, J. Juan-Alca ñiz, P. Serra-Crespo, M.W.G.M. Verhoeven, H. Niemantsverdriet, J. Gascon, F. Kapteijn, J. Catal. 289 (2012) 42.
[58] M.S. El-Shall, V. Abdelsayed, A.E.R.S. Khder, H.M.A. Hassan, H.M. El-Kaderi, T.E. Reich, J. Mater. Chem. 19 (2009) 7625.
[59] A. Aijaz, T. Akita, N. Tsumori, Q. Xu, J. Am. Chem. Soc. 135 (2013) 16356.
[60] W. Kleist, M. Maciejewski, A. Baiker, Thermochim. Acta 499 (2010) 71.
[61] J.M. Zamaro, N.C. Pérez, E.E. Miró, C. Casado, B. Seoane, C. Téllez, J. Coronas, Chem. Eng. J. 195-196 (2012) 180.
[62] F. Schröder, D. Esken, M. Cokoja, M.W.E. van den Berg, O.I. Lebedev, G. Van Tendeloo, B. Walaszek, G. Buntkowsky, H.-H. Limbach, B. Chaudret, R.A. Fischer, J. Am. Chem. Soc. 130 (2008) 6119.
[63] M. Müller, S. Turner, O.I. Lebedev, Y. Wang, G. van Tendeloo, R.A. Fischer, Eur. J. Inorg. Chem. 2011 (2011) 1876.
[64] T. Ishida, M. Nagaoka, T. Akita, M. Haruta, Chem.-Eur. J. 14 (2008) 8456.
[65] H. Liu, L. Chang, L. Chen, Y. Li, J. Mater. Chem. A 3 (2015) 8028.
[66] L. Chen, H. Chen, R. Luque, Y. Li, Chem. Sci. 5 (2014) 3708.
[67] H. Liu, Y. Liu, Y. Li, Z. Tang, H. Jiang, J. Phys. Chem. C 114 (2010) 13362.
[68] D. Esken, S. Turner, O.I. Lebedev, G. Van Tendeloo, R.A. Fischer, Chem. Mater. 22 (2010) 6393.
[69] K. Leus, P. Concepcion, M. Vandichel, M. Meledina, A. Grirrane, D. Esquivel, S. Turner, D. Poelman, M. Waroquier, V.V. Speybroeck, G.V. Tendeloo, H. García, P.V.D. Voort, RSC Adv. 5 (2015) 22334.
[70] Z. Sun, G. Li, L. Liu, H. Liu, Catal. Commun. 27 (2012) 200.
[71] J. Long, H. Liu, S. Wu, S. Liao, Y. Li, ACS Catal. 3 (2013) 647.
[72] X. Chen, N. Ding, H. Zang, H. Yeung, R.-S. Zhao, C. Cheng, J. Liu, T.-W.D. Chan, J. Chromatogr. A 1304 (2013) 241.
[73] Y. Huang, Y. Zhang, X. Chen, D. Wu, Z. Yi, R. Cao, Chem. Commun. 50 (2014) 10115.
[74] Q.-L. Zhu, J. Li, Q. Xu, J. Am. Chem. Soc. 135 (2013) 10210. [75]
P.-Z. Li, K. Aranishi, Q. Xu, Chem. Commun. 48 (2012) 3173. [76]
A.K. Singh, Q. Xu, ChemCatChem 5 (2013) 3000.
[77] X. Gu, Z.-H. Lu, H.-L. Jiang, T. Akita, Q. Xu, J. Am. Chem. Soc. 133 (2011) 11822.
[78] M. Martis, K. Mori, K. Fujiwara, W.-S. Ahn, H. Yamashita, J. Phys. Chem. C 117 (2013) 22805.
[79] M. Wen, K. Mori, T. Kamegawa, H. Yamashita, Chem. Commun. 50 (2014) 11645.
[80] C. Wang, K.E. deKrafft, W. Lin, J. Am. Chem. Soc. 134 (2012) 7211.
[81] Y. Horiuchi, T. Toyao, M. Saito, K. Mochizuki, M. Iwata, H. Higashimura, M. Anpo, M. Matsuoka, J. Phys. Chem. C 116 (2012) 20848.
[82] A. Henschel, K. Gedrich, R. Kraehnert, S. Kaskel, Chem. Commun. 45 (2008) 4192.
[83] P. Wang, J. Zhao, X. Li, Y. Yang, Q. Yang, C. Li, Chem. Commun. 49 (2013) 3330.
[84] C.J. Stephenson, J.T. Hupp, O.K. Farha, Inorg. Chem. 2 (2015) 448.

[85] H. Pan, X. Li, D. Zhang, Y. Guan, P. Wu, J. Mol. Catal. Chem. 377 (2013) 108.
[86] J. Hermannsdörfer, M. Friedrich, R. Kempe, Chem.-Eur. J. 19 (2013) 13652.
[87] D. Zhang, Y. Guan, E.J.M. Hensen, L. Chen, Y. Wang, Catal. Commun. 41 (2013) 47.
[88] W. Du, G. Chen, R. Nie, Y. Li, Z. Hou, Catal. Commun. 41 (2013) 56.
[89] J. Hermannsdörfer, R. Kempe, Chem.-Eur. J. 17 (2011) 8071.
[90] H. Khajavi, H.A. Stil, H.P.C.E. Kuipers, J. Gascon, F. Kapteijn, ACS Catal. 3 (2013) 2617.
[91] X. Zhao, Y. Jin, F. Zhang, Y. Zhong, W. Zhu, Chem. Eng. J. 239 (2014) 33.
[92] Y. Huang, S. Liu, Z. Lin, W. Li, X. Li, R. Cao, J. Catal. 292 (2012) 111.
[93] B. Yuan, Y. Pan, Y. Li, B. Yin, H. Jiang, Angew. Chem. Int. Ed. 49 (2010) 4054.
[94] Y. Huang, Z. Zheng, T. Liu, J. Lü, Z. Lin, H. Li, R. Cao, Catal. Commun. 14 (2011) 27.
[95] V. Pascanu, Q. Yao, A. Bermejo Gómez, M. Gustafsson, Y. Yun, W. Wan, L. Samain, X. Zou, B. Martín-Matute, Chem.-Eur. J. 19 (2013) 17483.
[96] A.S. Roy, J. Mondal, B. Banerjee, P. Mondal, A. Bhaumik, S.M. Islam, Appl. Catal. Gen. 469 (2014) 320.
[97] S. Gao, N. Zhao, M. Shu, S. Che, Appl. Catal. Gen. 388 (2010) 196.
[98] Y. Huang, S. Gao, T. Liu, J. Lü, X. Lin, H. Li, R. Cao, ChemPlusChem 77 (2012) 106.
[99] A. Aijaz, A. Karkamkar, Y.J. Choi, N. Tsumori, E. Rönnebro, T. Autrey, H. Shioyama, Q. Xu, J. Am. Chem. Soc. 134 (2012) 13926.
[100] J.Y. Kim, M. Jin, K.J. Lee, J.Y. Cheon, S.H. Joo, J.M. Kim, H.R. Moon, Nanoscale Res. Lett. 7 (2012) 461.
[101] Y. Luan, Y. Qi, H. Gao, N. Zheng, G. Wang, J. Mater. Chem. A 2 (2014) 20588.
[102] J. Zhu, P.C. Wang, M. Lu, Appl. Catal. Gen. 477 (2014) 125.
[103] G. Chen, S. Wu, H. Liu, H. Jiang, Y. Li, Green Chem. 15 (2012) 230.
[104] M. Zhang, Y. Yang, C. Li, Q. Liu, C.T. Williams, C. Liang, Catal. Sci. Technol. 4 (2014) 329.
[105] T.-H. Park, A.J. Hickman, K. Koh, S. Martin, A.G. Wong-Foy, M.S. Sanford, A.J. Matzger, J. Am. Chem. Soc. 133 (2011) 20138.
[106] Z. Li, H.C. Zeng, Chem. Mater. 25 (2013) 1761.
[107] H.-L. Jiang, T. Akita, T. Ishida, M. Haruta, Q. Xu, J. Am. Chem. Soc. 133 (2011) 1304.
[108] F. Ke, J. Zhu, L.-G. Qiu, X. Jiang, Chem. Commun. 49 (2013) 1267.
[109] J. Hermannsdörfer, M. Friedrich, N. Miyajima, R.Q. Albuquerque, S. Kümmel, R. Kempe, Angew. Chem. Int. Ed. 51 (2012) 11473.
[110] Y. Zhao, J. Zhang, J. Song, J. Li, J. Liu, T. Wu, P. Zhang, B. Han, Green Chem. 13 (2011) 2078.
[111] Y. Liu, W. Zhang, S. Li, C. Cui, J. Wu, H. Chen, F. Huo, Chem. Mater. 26 (2014) 1119.
[112] A. Aijaz, Q.-L. Zhu, N. Tsumori, T. Akita, Q. Xu, Chem. Commun. 51 (2015) 2577.
[113] M. Gulcan, M. Zahmakiran, S. Özkar, Appl. Catal. B Environ. 147 (2014) 394.
[114] L. Shen, W. Wu, R. Liang, R. Lin, L. Wu, Nanoscale 5 (2013) 9374.
[115] M. Yadav, Q. Xu, Chem. Commun. 49 (2013) 3327.
[116] M. Müller, S. Hermes, K. Kähler, M.W.E. van den Berg, M. Muhler, R.A. Fischer, Chem. Mater. 20 (2008) 4576.
[117] K. Na, K.M. Choi, O.M. Yaghi, G.A. Somorjai, Nano Lett. 14 (2014) 5979.
[118] F.G. Cirujano, A. Leyva-Pérez, A. Corma, F.X. LlabrésiXamena, ChemCatChem 5 (2013) 538.
[119] T.T. Dang, Y. Zhu, J.S.Y. Ngiam, S.C. Ghosh, A. Chen, A.M. Seayad, ACS Catal. 3 (2013) 1406.
[120] T.T. Dang, Y. Zhu, S.C. Ghosh, A. Chen, C.L.L. Chai, A.M. Seayad, Chem. Commun. 48 (2012) 1805.
[121] H. Li, Z. Zhu, F. Zhang, S. Xie, H. Li, P. Li, X. Zhou, ACS Catal. 1 (2011) 1604.
[122] Y.K. Park, S.B. Choi, H.J. Nam, D.-Y. Jung, H.C. Ahn, K. Choi, H. Furukawa, J. Kim, Chem. Commun. 46 (2010) 3086.
[123] Y. Huang, Z. Lin, R. Cao, Chem.-Eur. J. 17 (2011) 12706.
[124] L. Rimai, J.H. Visser, E.M. Logothetis, A. Samman, in: Polym. Sens., American Chemical Society, 1998, p. 102.
[125] D. Wencel, T. Abel, C. McDonagh, Anal. Chem. 86 (2014) 15.
[126] S. Joo, R.B. Brown, Chem. Rev. 108 (2008) 638.
[127] F. Xiao, J. Song, H. Gao, X. Zan, R. Xu, H. Duan, ACS Nano 6 (2012) 100.
[128] M. Segev-Bar, H. Haick, ACS Nano 7 (2013) 8366.
[129] L.E. Kreno, K. Leong, O.K. Farha, M. Allendorf, R.P. Van Duyne, J.T. Hupp, Chem. Rev. 112 (2012) 1105.
[130] J. Lei, R. Qian, P. Ling, L. Cui, H. Ju, TrAC Trends Anal. Chem. 58 (2014) 71.
[131] M. Dincă, J.R. Long, J. Am. Chem. Soc. 127 (2005) 9376.
[132] B. Sharma, R.R. Frontiera, A.-I. Henry, E. Ringe, R.P. Van Duyne, Mater. Today 15 (2012) 16.
[133] M. Schierhorn, S.J. Lee, S.W. Boettcher, G.D. Stucky, M. Moskovits, Adv. Mater. 18 (2006) 2829.
[134] Y. Sawai, B. Takimoto, H. Nabika, K. Ajito, K. Murakoshi, J. Am. Chem. Soc. 129 (2007) 1658.
[135] Y. Zhao, N. Kornienko, Z. Liu, C. Zhu, S. Asahina, T.-R. Kuo, W. Bao, C. Xie, A. Hexemer, O. Terasaki, P. Yang, O.M. Yaghi, J. Am. Chem. Soc. 137 (2015) 2199.
[136] Z. Xu, L. Yang, C. Xu, Anal. Chem. 87 (2015) 3438.
[137] W. Zhan, Q. Kuang, J. Zhou, X. Kong, Z. Xie, L. Zheng, J. Am. Chem. Soc. 135 (2013) 1926.
[138] D. Buso, J. Jasieniak, M.D.H. Lay, P. Schiavuta, P. Scopece, J. Laird, H. Amenitsch, A.J. Hill, P. Falcaro, Small 8 (2012) 80.
[139] P. Falcaro, F. Normandin, M. Takahashi, P. Scopece, H. Amenitsch, S. Costacurta, C.M. Doherty, J.S. Laird, M.D.H. Lay, F. Lisi, A.J. Hill, D. Buso, Adv. Mater. 23 (2011) 3901.
[140] J.-R. Li, J. Sculley, H.-C. Zhou, Chem. Rev. 112 (2012) 869.
[141] L. He, Y. Liu, J. Liu, Y. Xiong, J. Zheng, Y. Liu, Z. Tang, Angew. Chem. Int. Ed. 52 (2013) 3741.
[142] D. Zhao, X. Wan, H. Song, L. Hao, Y. Su, Y. Lv, Sens. Actuators B Chem. 197 (2014) 50.
[143] G. Lu, J.T. Hupp, J. Am. Chem. Soc. 132 (2010) 7832.
[144] P. Innocenzi, L. Malfatti, P. Falcaro, Water Droplets to Nanotechnology, RSC Publishing, Cambridge, UK, 2013.
[145] O. Shekhah, H. Wang, S. Kowarik, F. Schreiber, M. Paulus, M. Tolan, C. Sternemann, F. Evers, D. Zacher, R.A. Fischer, C. Wöll, J. Am. Chem. Soc. 129 (2007) 15118.
[146] G. Lu, O.K. Farha, L.E. Kreno, P.M. Schoenecker, K.S. Walton, R.P. Van Duyne, J.T. Hupp, Adv. Mater. 23 (2011) 4449.
[147] Y. Wu, F. Li, Y. Xu, W. Zhu, C. Tao, J. Cui, G. Li, Chem. Commun. 47 (2011) 10094.
[148] R. Ameloot, M.B.J. Roeffaers, G. De Cremer, F. Vermoortele, J. Hofkens, B.F. Sels, D.E. De Vos, Adv. Mater. 23 (2011) 1788.
[149] Y. Wu, F. Li, W. Zhu, J. Cui, C. Tao, C. Lin, P.M. Hannam, G. Li, Angew. Chem. Int. Ed. 50 (2011) 12518.
[150] R. Ameloot, E. Gobechiya, H. Uji-i, J.A. Martens, J. Hofkens, L. Alaerts, B.F. Sels, D.E. De Vos, Adv. Mater. 22 (2010) 2685.
[151] C. Cui, Y. Liu, H. Xu, S. Li, W. Zhang, P. Cui, F. Huo, Small 10 (2014) 3672.
[152] F.M. Hinterholzinger, A. Ranft, J.M. Feckl, B. Rühle, T. Bein, B.V. Lotsch, J. Mater. Chem. 22 (2012) 10356.
[153] Z. Hu, C. Tao, F. Wang, X. Zou, J. Wang, J. Mater. Chem. C 3 (2015) 211.
[154] A. Ranft, F. Niekiel, I. Pavlichenko, N. Stock, B.V. Lotsch, Chem. Mater. 27 (2015) 1961.
[155] G. Lu, O.K. Farha, W. Zhang, F. Huo, J.T. Hupp, Adv. Mater. 24 (2012) 3970.
[156] J. Liu, E. Redel, S. Walheim, Z. Wang, V. Oberst, J. Liu, S. Heissler, A. Welle, M. Moosmann, T. Scherer, M. Bruns, H. Gliemann, C. Wöll, Chem. Mater. 27 (2015) 1991.
[157] J. Cui, N. Gao, C. Wang, W. Zhu, J. Li, H. Wang, P. Seidel, B.J. Ravoo, G. Li, Nanoscale 6 (2014) 11995.
[158] E. Zanchetta, L. Malfatti, R. Ricco, M.J. Styles, F. Lisi, C.J. Coghlan, C.J. Doonan, A.J. Hill, G. Brusatin, P. Falcaro, Chem. Mater. 27 (2015) 690.
[159] Q.-R. Fang, D.-Q. Yuan, J. Sculley, J.-R. Li, Z.-B. Han, H.-C. Zhou, Inorg. Chem. 49 (2010) 11637.
[160] E. Tahmasebi, M.Y. Masoomi, Y. Yamini, A. Morsali, Inorg. Chem. 54 (2015) 425.
[161] X. Zhu, B. Li, J. Yang, Y. Li, W. Zhao, J. Shi, J. Gu, ACS Appl. Mater. Interfaces 7 (2015) 223.
[162] M. Majumder, P. Sheath, J.I. Mardel, T.G. Harvey, A.W. Thornton, A. Gonzago, D.F. Kennedy, I. Madsen, J.W. Taylor, D.R. Turner, M.R. Hill, Chem. Mater. 24 (2012) 4647.
[163] C.W. Abney, K.M.L. Taylor-Pashow, S.R. Russell, Y. Chen, R. Samantaray, J.V. Lockard, W. Lin, Chem. Mater. 26 (2014) 5231.
[164] J.B. DeCoste, G.W. Peterson, Chem. Rev. 114 (2014) 5695.
[165] R. Ricco, L. Malfatti, M. Takahashi, A.J. Hill, P. Falcaro, J. Mater. Chem. A 1 (2013) 13033.
[166] M.R. Lohe, K. Gedrich, T. Freudenberg, E. Kockrick, T. Dellmann, S. Kaskel, Chem. Commun. 47 (2011) 3075.
[167] C.M. Doherty, E. Knystautas, D. Buso, L. Villanova, K. Konstas, A.J. Hill, M. Takahashi, P. Falcaro, J. Mater. Chem. 22 (2012) 11470.
[168] S.-H. Huo, X.-P. Yan, Analyst 137 (2012) 3445.
[169] A. Carné-Sánchez, I. Imaz, M. Cano-Sarabia, D. Maspoch, Nat. Chem. 5 (2013) 203.
[170] L. Järup, Br. Med. Bull. 68 (2003) 167.
[171] G.W. Bryan, W.J. Langston, Environ. Pollut. 76 (1992) 89.
[172] M.R. Sohrabi, Z. Matbouie, A.A. Asgharinezhad, A. Dehghani, Microchim. Acta 180 (2013) 589.
[173] Y. Wang, J. Xie, Y. Wu, H. Ge, X. Hu, J. Mater. Chem. A 1 (2013) 8782.
[174] M. Taghizadeh, A.A. Asgharinezhad, M. Pooladi, M. Barzin, A. Abbaszadeh, A. Tadjarodi, Microchim. Acta 180 (2013) 1073.
[175] P. Falcaro, F. Lapierre, B. Marmiroli, M. Styles, Y. Zhu, M. Takahashi, A.J. Hill, C.M. Doherty, J. Mater. Chem. C 1 (2012) 42.
[176] A. Bagheri, M. Taghizadeh, M. Behbahani, A. Akbar Asgharinezhad, M. Salarian, A. Dehghani, H. Ebrahimzadeh, M.M. Amini, Talanta 99 (2012) 132.
[177] E.I. Cedillo-González, R. Riccò, M. Montorsi, M. Montorsi, P. Falcaro, C. Siligardi, Build. Environ. 71 (2014) 7.
[178] M. Pelaez, N.T. Nolan, S.C. Pillai, M.K. Seery, P. Falaras, A.G. Kontos, P.S.M. Dunlop, J.W.J. Hamilton, J.A. Byrne, K. O'Shea, M.H. Entezari, D.D. Dionysiou, Appl. Catal. B Environ. 125 (2012) 331.
[179] Y. Hu, Z. Huang, L. Zhou, D. Wang, G. Li, J. Sep. Sci. 37 (2014) 1482.
[180] T. Zeng, X. Zhang, S. Wang, H. Niu, Y. Cai, Environ. Sci. Technol. 49 (2015) 2350.
[181] Z. Zhang, Y. Chen, X. Xu, J. Zhang, G. Xiang, W. He, X. Wang, Angew. Chem. Int. Ed. 53 (2014) 429.
[182] Z.-Y. Gu, C.-X. Yang, N. Chang, X.-P. Yan, Acc. Chem. Res. 45 (2012) 734.
[183] M. Palomino, A. Cant?n, A. Corma, S. Leiva, F. Rey, S. Valencia, Chem. Commun. (2007) 1233.
[184] M.E. Silvestre, M. Franzreb, P.G. Weidler, O. Shekhah, C. Wöll, Adv. Funct. Mater. 23 (2013) 1210.
[185] R.C. Huxford, J. Della Rocca, W. Lin, Curr. Opin. Chem. Biol. 14 (2010) 262.
[186] P. Horcajada, R. Gref, T. Baati, P.K. Allan, G. Maurin, P. Couvreur, G. Férey, R.E. Morris, C. Serre, Chem. Rev. 112 (2012) 1232.
[187] P. Horcajada, T. Chalati, C. Serre, B. Gillet, C. Sebrie, T. Baati, J.F. Eubank, D. Heurtaux, P. Clayette, C. Kreuz, J.-S. Chang, Y.K. Hwang, V. Marsaud, P.-N. Bories, L. Cynober, S. Gil, G. Férey, P. Couvreur, R. Gref, Nat. Mater. 9 (2010) 172.

[188] D. Cunha, M. Ben Yahia, S. Hall, S.R. Miller, H. Chevreau, E. Elkaïm, G. Maurin, P. Horcajada, C. Serre, Chem. Mater. 25 (2013) 2767.
[189] T. Kundu, S. Mitra, P. Patra, A. Goswami, D. Díaz Díaz, R. Banerjee, Chem.-Eur. J. 20 (2014) 10514.
[190] X. Zhu, J. Gu, Y. Wang, B. Li, Y. Li, W. Zhao, J. Shi, Chem. Commun. 50 (2014) 8779.
[191] J.W. Brown, B.L. Henderson, M.D. Kiesz, A.C. Whalley, W. Morris, S. Grunder, H. Deng, H. Furukawa, J.I. Zink, J.F. Stoddart, O.M. Yaghi, Chem. Sci. 4 (2013) 2858.
[192] L. Heinke, M. Cakici, M. Dommaschk, S. Grosjean, R. Herges, S. Bräse, C. Wöll, ACS Nano 8 (2014) 1463.
[193] R.K. Deshpande, G.I.N. Waterhouse, G.B. Jameson, S.G. Telfer, Chem. Commun. 48 (2012) 1574.
[194] S. Diring, D.O. Wang, C. Kim, M. Kondo, Y. Chen, S. Kitagawa, K. Kamei, S. Furukawa, Nat. Commun. 4 (2013).
[195] F. Ke, Y.-P. Yuan, L.-G. Qiu, Y.-H. Shen, A.-J. Xie, J.-F. Zhu, X.-Y. Tian, L.-D. Zhang, J. Mater. Chem. 21 (2011) 3843.
[196] P. Küsgens, M. Rose, I. Senkovska, H. Fröde, A. Henschel, S. Siegle, S. Kaskel, Microporous Mesoporous Mater. 120 (2009) 325.
[197] Y. Wu, M. Zhou, S. Li, Z. Li, J. Li, B. Wu, G. Li, F. Li, X. Guan, Small 10 (2014) 2927.
[198] X. Qian, B. Yadian, R. Wu, Y. Long, K. Zhou, B. Zhu, Y. Huang, Int. J. Hydrog. Energy 38 (2013) 16710.
[199] X. Wang, G. Li, Y. Ding, S. Sun, RSC Adv. 4 (2014) 30375.
[200] X.-L. Liu, R. Wang, M.-Y. Zhang, Y.-P. Yuan, C. Xue, APL Mater. 3 (2015) 104403.
[201] Y. Li, J. Tang, L. He, Y. Liu, Y. Liu, C. Chen, Z. Tang, Adv. Mater. (2015) 4075.